2-oxoglutarate triggers assembly of active dodecameric *Methanosarcina mazei* glutamine synthetase

Eva Herdering[1], Tristan Reif-Trauttmansdorff[2], Anuj Kumar[2], Tim Habenicht[1], Georg Hochberg[2, 3, 4], Stefan Bohn[5], Jan Schuller[2], and Ruth A. Schmitz[1]

[1] Institute for General Microbiology, Christian Albrechts University, Am Botanischen Garten 1-9, D-24118 Kiel, Germany;
[2] Center for Synthetic Microbiology (SYNMIKRO) Research Center and Department of Chemistry, Philipps-Universität Marburg, Karl-von-Frisch Straße 14, 35043 Marburg
[3] Evolutionary Biochemistry Group, Max Planck Institute for Terrestrial Microbiology, Marburg, Karl-von-Frisch Straße 10, 35043 Marburg
[4] Department of Chemistry, Philipps-Universität Marburg, Hans-Meerwein-Straße 4, 35043 Marburg
[5] Institute of Structural Biology, Helmholtz Zentrum Munich, Ingolstädter Landstrasse 1, 85764 Neuherberg, Germany

* Correspondence: **Ruth Anne Schmitz**
rschmitz@ifam.uni-kiel.de, phone: +49-(0)431-880-4334

Abstract

Glutamine synthetases (GS) are central enzymes essential for the nitrogen metabolism across all domains of life. Consequently, they have been extensively studied for more than half a century. Based on the ATP dependent ammonium assimilation generating glutamine, GS expression and activity are strictly regulated in all organisms. In the methanogenic archaeon *Methanosarcina mazei*, it has been shown that the metabolite 2-oxoglutarate (2-OG) directly induces the GS activity. Besides, modulation of the activity by interaction with small proteins ($GlnK_1$ and sP26) has been reported. Here, we show that the strong activation of *M. mazei* GS ($GlnA_1$) by 2-OG is based on the 2-OG dependent dodecamer assembly of $GlnA_1$ by using mass photometry (MP) and single particle cryo-electron microscopy (cryo-EM) analysis of purified strep-tagged $GlnA_1$. The dodecamer assembly from monomers/dimers occurred without any detectable intermediate oligomeric state and was not affected in the presence of $GlnK_1$. The 2.39 Å cryo-EM structure of the dodecameric complex in the presence of 12.5 mM 2-OG demonstrated that 2-OG is binding between two monomers. Thereby, 2-OG appears to induce the dodecameric assembly in a cooperative way. Furthermore, the active site is primed by an allosteric interaction cascade caused by 2-OG-binding towards an adaption of the transition state catalytic conformation. In the presence of additional glutamine, strong feedback inhibition of GS activity was observed. Since glutamine dependent disassembly of the dodecamer was excluded by MP, feedback inhibition most likely relies on an allosteric binding of glutamine to the catalytic site. Based on our findings, we propose that under nitrogen limitation the induction of *M. mazei* GS into a catalytically active dodecamer is not affected by $GlnK_1$ and crucially depends on the presence of 2-OG.

55 **Introduction**

56 Nitrogen is one of the key elements in life and it is essentially required in form of ammonium for
57 biomolecules such as proteins or nucleic acids. Two major pathways of ammonium assimilation in
58 bacteria and archaea are known. Under nitrogen (N) sufficiency glutamate dehydrogenase (GDH) is
59 active and generates glutamate from oxoglutarate and ammonium (reviewed in van Heeswijk et al.,
60 2013). However, under N limitation low ammonium concentrations lead to inactive GDH as a result
61 of its low ammonium affinity, whereas the expression of glutamine synthetase (GS) is strongly
62 induced in response to N limitation (Bolay et al., 2018; Gunka and Commichau, 2012; Stadtman,
63 2001). Consequently, under low ammonium conditions GS together with glutamate synthase
64 (GOGAT) are responsible for ammonium assimilation via the GS/GOGAT pathway, one of the major
65 intersections in central carbon and N metabolism. Accordingly, GS present across all domains of life
66 plays a central role in cellular N assimilation under low N availability. The enzyme, its structure and
67 regulation has been investigated in detail in different organisms for more than half a century (e.g.
68 Dos Santos Moreira et al., 2019; Stadtman, 2001; Woolfolk and Stadtman, 1967).

69 Most of the GS are grouped into three major classes based on their monomeric size and
70 oligomerization properties (overview in Dos Santos Moreira et al., 2019). GSI and GSIII, both found in
71 bacteria and archaea mostly form dodecamers, whereas GSII found in Eukaryotes form decamers of
72 smaller subunits (Dos Santos Moreira et al., 2019; He et al., 2009; Valentine et al., 1968; van Rooyen
73 et al., 2011). The GSI class can be further grouped into Iα-type GS and Iβ-type GS based on their
74 amino acid sequence and respective molecular mechanisms of activity regulation. Iß-type GS contain
75 a conserved adenylylation site (Tyr397 residue near the active site) that allows for covalent
76 modification of Iβ-type GS and leads to inactivation of the enzyme (Brown et al., 1994; Magasanik,
77 1993; Shapiro and Stadtman, 1970), whereas Iα-type GS are not covalently modified and mainly
78 show feedback inhibition by end products of the glutamine metabolism including glutamine (Fisher,
79 1999; Gunka and Commichau, 2012).

80 *GS regulation on transcriptional level*

81 Since in contrast to GDH, GS catalyzed generation of glutamine requires ATP, most organisms strictly
82 regulate the expression of GS in response to the nitrogen availability on the transcriptional level. In
83 gram negative bacteria mainly transcriptional activation of the coding gene (*glnA*) under low nitrogen
84 availability occurs via a transcriptional activator (e.g. NtrC in *Escherichia coli* (Jiang et al., 1998)). For
85 several gram positive bacteria however, the mechanism of regulation is a de-repression of *glnA*
86 transcription under N limitation, which has also been shown for methanoarchaea (Cohen-Kupiec et
87 al., 1999; Fedorova et al., 2013; Fisher, 1999; Fisher and Wray, 2008; Hauf et al., 2016; Weidenbach
88 et al., 2010, 2008). Whereas in gram positives the signal perception is complex and often also

involves protein interactions of GS with transcriptional regulators (reviewed in Gunka and Commichau, 2012), signal perception and transduction in methanoarchaea occurs directly via the small effector molecule 2-oxoglutarate (2-OG), which increases under N limitation. It has been shown that binding of 2-OG to the global N repressor protein NrpR significantly changes the repressor conformation resulting in dissociation from its respective operator (Lie et al., 2007; Weidenbach et al., 2010; Wisedchaisri et al., 2010). In addition to expression regulation the activity of GS is also strictly regulated in all organisms in response to changing N availabilities, however the underlying molecular mechanism(s) of inhibition significantly differ for the various GS classes and in various organisms (Reitzer, 2003)

Regulation of GS activity: highly diverse and often complex in various organisms

An extensive repertoire of cellular control mechanisms regulating GS activity in response to N availability has been observed in different organisms. Inhibitory mechanisms in response to an N upshift range from feedback inhibition by e.g. glutamine or other end products of the glutamine metabolism (e.g. *E. coli* (Stadtman, 2004), *Bacillus subtilis* (Deuel et al., 1970), yeast (Legrain et al., 1982)), proteolytic degradation (yeast, (Legrain et al., 1982), covalent modification by adenylylation of the 1ß-type GS subunits (e.g. enterobacteriaceae), thiol-based GS regulation (e.g. in soybean nodules (Masalkar and Roberts, 2015)), inhibition by regulatory proteins (e.g. in gram positive bacteria (Travis et al., 2022a)), inhibition by interactions with small proteins (e.g. inhibitory factors in Cyanobacteria (García-Domínguez et al., 1999; Klähn et al., 2018, 2015)), to directly effecting the activity through the presence or absence of the small metabolite 2-OG, which has been shown for the first time for *Methanosarcina mazei* (Ehlers et al., 2005). Moreover, often complex regulations for GS activity including several of the different regulatory mechanisms are reported for one organism. For example, yeast GS (ScGS) is regulated via feedback inhibition by glutamine and is susceptible to proteolytic degradation under N starvation. It was also found to assemble into nanotubes (He et al., 2009) and under advanced cellular starvation into inactive filaments (Petrovska et al., 2014). In *E. coli*, the activity of the Iß-type GS (EcGS) is controlled by cumulative feedback inhibition and covalent modification (reviewed in Reitzer, 2003). It has been shown that each of the 12 subunits can be modified by adenylylation (Tyr397) resulting in an inactivation of the respective subunit (Stadtman, 1990). Moreover, the adenlylylation of single subunits in the complex in addition makes the other subunits more susceptible to cumulative feedback inhibition by various substances (Stadtman, 1990). These substances either bind the glutamine-binding pocket or have an allosteric binding site (Liaw et al., 1993; Woolfolk and Stadtman, 1967). The dodecameric structure of EcGS has been known for a long time (Almassy et al., 1986; Yamashita et al., 1989). However, when artificially exposed to divalent cations (Mn^{2+}, Co^{2+}) it randomly aggregates and produces long hexagonal tubes (paracrystalline aggregates) (Valentine et al., 1968). The detailed structural information on the

124 mechanisms of this GS-filament formation to an inactive form of EcGS, often associated with stress
125 responses, as well as the reversion into individual active dodecamers has only recently been
126 described by cryo-electron microscopy (cryo-EM) analysis (Huang et al., 2022). The *B. subtilis* GS has
127 been shown to be feedback regulated. In addition, binding of the transcriptional repressor GlnR to
128 the feedback inhibited complex not only activates the transcription repression function of GlnR
129 (Fisher and Wray, 2008) but also stabilizes the inactive GS conformation potentially changing from a
130 dodecamer into a tetradecameric structure (Travis et al., 2022a).

131 In *M. mazei,* a mesophilic methanoarchaeon, which is able to fix N_2, regulation of the central N
132 metabolisms has been studied extensively on the transcriptional and post-transcriptional level (Jäger
133 et al., 2009; Prasse and Schmitz, 2018; Veit et al., 2005). A central role of 2-OG for the perception of
134 changes in N availabilities has been proposed as has been demonstrated for cyanobacteria
135 (Forchhammer, 1999; Herrero et al., 2001). The activity of *M. mazei* GS encoded by *glnA$_1$*, is
136 regulated by several different mechanisms. GS /$GlnA_1$) is not covalently modified in response to N
137 availability and thus represents a Iß-type-GS (Ehlers et al., 2005). It has been demonstrated to get
138 directly activated under N starvation due to the high intracellular concentrations of the metabolite 2-
139 OG which directly induces $GlnA_1$ activity (Ehlers et al., 2005). 2-OG represents the internal signal for
140 N limitation since under N starvation the internal 2-OG level significantly increases due to missing
141 consumption by GDH (*M. mazei* contains the oxidative TCA part, anabolic). The increased cellular 2-
142 OG concentration has been shown to be directly perceived by the $GlnA_1$ most likely by direct binding
143 resulting in strong activation (Ehlers et al., 2005). Besides, we showed first evidence that in addition
144 two small proteins interact with *M. mazei* $GlnA_1$, the PII-like protein $GlnK_1$ and small protein sP26
145 comprising 23 amino acids (Ehlers et al., 2005; Gutt et al., 2021). The presence and potential
146 interaction of both small proteins show small effects on the $GlnA_1$ activity, however compared to the
147 strong 2-OG stimulation only to a very low extend, which might be neglectable and due to the
148 indirect GS activity assay. Moreover, based on initial complex formation analysis using size exclusion
149 chromatography (SEC) and pull-down approaches first indications were obtained that in the absence
150 of 2-OG the $GlnA_1$/$GlnK_1$ complexes are more stable than in the presence of high 2-OG. This led to
151 the conclusion that due to the shift to N sufficiency after a period of N limitation, $GlnA_1$ activity is
152 reduced due to the lower 2-OG concentration but also due to the inhibitory protein interaction with
153 $GlnK_1$ (Ehlers et al., 2005). Very recently the first structural analysis of *M. mazei* $GlnA_1$ was reported,
154 showing first GS complexes with $GlnK_1$ (Schumacher et al. 23). Based on their findings Schumacher et
155 al. propose a regulation of $GlnA_1$ activity by oligomeric modulation, with $GlnK_1$ stabilizing the
156 dodecameric structure and the formation of $GlnA_1$ active sites. Since this proposed model is entirely
157 missing the effects of 2-OG on $GlnA_1$ activity, we here aimed to study the obtained effects regulating
158 *M. mazei* $GlnA_1$ activity in more detail by evaluating oligomerization and complex formation between

159 $GlnA_1$, $GlnK_1$ and sP26 in dependence of 2-OG employing mass photometry (MP) allowing molecular
160 weight distribution of single complexes in solution and by high resolution cryo-EM.

161

162 RESULTS

163 *2-OG is responsible for $GlnA_1$-dodecamer formation in* M. mazei

164 The strep-tagged purified $GlnA_1$ was analyzed by SEC in the presence of 12.5 mM 2-OG
165 demonstrating that GS is exclusively present in a dodecameric structure, no other oligomers were
166 detectable (suppl. Fig. S1). To investigate the effects of 2-OG on *M. mazei* $GlnA_1$ in more detail, we
167 employed MP, a method that allows to measure the molecular weight distribution in solution. Strep-
168 tagged purified $GlnA_1$ (after SEC) was dialyzed into a 2-OG free HEPES buffer (see Materials and
169 Methods) and subsequently analyzed by MP, demonstrating that in the presence of low 2-OG
170 concentrations (0.1 mM) all of the *M. mazei* $GlnA_1$ was exclusively present as monomers/dimers with
171 no higher molecular weight complexes present. After addition of 12.5 mM 2-OG, the size distribution
172 shifted towards a higher molecular weight complex of 630-700 kDa (calculated based on the
173 measured dimer-size in each measurement; expected molecular weight of dodecamer: 634 kDa) (Fig.
174 1A, B). This molecular weight corresponds to a fully assembled dodecamer species, the same
175 oligomeric structure that is adapted in GS from other prokaryotes. Using 2-OG concentrations varying
176 between 0.1 and 12.5 mM, complex analysis showed that up to 62 % of all particles were assembled
177 in a dodecamer. This further allowed to determine the binding affinity of $GlnA_1$ to 2-OG to be K_D =
178 0.75 ± 0.01 mM 2-OG (based on two biological replicates, calculated with the percentage of
179 dodecamer) as described in Materials and Methods, and verified that no other intermediate
180 oligomeric complexes were detectable during dodecameric assembly (Fig. 1A, C, suppl. Fig. S2A, B).
181 Activity measurements of Strep-$GlnA_1$ in the presence of increasing 2-OG concentrations showed a
182 strong increase of the activity from 0.0 U/mg in the absence of 2-OG up to 7.8 ± 1.7 U/mg in the
183 presence of 12.5 mM 2-OG (six independent protein purifications, Fig. 1D). Thus, we conclude that 2-
184 OG acts as a trigger for dodecameric assembly of *M. mazei* $GlnA_1$, setting it apart from other bacterial
185 and eukaryotic enzyme variants. Moreover, most likely in addition to the dodecameric assembly, 2-
186 OG is additionally required for a further 2-OG induced conformational switch of the active site, since
187 saturated $GlnA_1$ activities are not reached in the presence of 5 mM 2-OG, when most of the $GlnA_1$ is
188 in a dodecameric structure. For full activity, the presence of 12.5 mM 2-OG is required.

189 **Figure 1**

190

191 *$GlnK_1$ has no detectable effects on GS dodecamer assembly or activity under the tested conditions*

192 Previous studies have shown protein interactions between *M. mazei* $GlnA_1$ and $GlnK_1$ as well as $GlnK_1$
193 induced effects on $GlnA_1$ activity. Consequently, we next tested the effects of $GlnK_1$ presence on the
194 $GlnA_1$ oligomerization in the presence of 2-OG. Performing the MP analysis under the tested
195 conditions as before but in the presence of purified $GlnK_1$ demonstrated that (i) in the absence of 2-
196 OG varying ratios between $GlnA_1$ and $GlnK_1$ (20:1, 2:1, 2:10 based on monomers) did not result in any
197 dodecamer assembly of $GlnA_1$ (Fig. 2A, B), (ii) no difference in the $GlnA_1$ dodecameric assembly in the
198 presence of 2-OG was obtained in the presence of purified $GlnK_1$ (2:1), (iii) nor was binding of $GlnK_1$
199 to $GlnA_1$ detected by a respective increase in the mass of the higher oligomeric complex (Fig. 2B, C).
200 Moreover, the presence of $GlnK_1$ (2:1) neither had an influence on the 2-OG affinity (K_D (- $GlnK_1$) =
201 1.06 mM 2-OG; K_D (+ $GlnK_1$) = 1.02 mM 2-OG, K_D calculated based on the dodecamer/dimer ratio),
202 nor in any ratio on the specific activity of $GlnA_1$ (Fig. 2 D, C: exemplarily showing 2:1; suppl. Fig. S2C,
203 D). Consequently, we conclude that under the conditions tested using purified proteins, $GlnA_1$
204 dodecamer assembly occurs independently of $GlnK_1$ and no binding of $GlnK_1$ to the dodecameric
205 $GlnA_1$ occurs. However, we cannot exclude that cellular components/metabolites not present in
206 these experiments are crucial for a $GlnA_1$-$GlnK_1$ interaction.

207 **Figure 2**

208

209 *Structural basis of oligomer formation by 2-OG*

210 To now unravel the structural mechanism underlying *M. mazei* $GlnA_1$ activation by 2-OG, we
211 employed cryo-EM and single-particle analysis. Treating freshly purified Strep-$GlnA_1$ with 12.5 mM 2-
212 OG, effectively shifted the equilibrium towards fully assembled homo-oligomers as depicted in the
213 MP experiments. In the micrographs, fully assembled ring-shaped particles are visible. However,
214 initial attempts to obtain a 3D reconstruction were hindered by the pronounced preferred
215 orientation of particles within the ice, a challenge which has been overcome by introducing low
216 concentrations of CHAPSO (0.7 mM). In our final dataset, all particles exhibited well-distributed
217 oligomers in diverse orientations. Leveraging this dataset, we aligned the particles to a 2.39 Å
218 resolution structure, revealing well resolved side chains that facilitated seamless model building (Fig.
219 3, suppl. Fig. S3, suppl. Tab. S2). Consequently, we achieved a structure demonstrating excellent
220 geometry and density fitting.

221 The detailed structural analysis uncovered that $GlnA_1$ assembles into a dodecamer characterized by
222 stacked hexamer rings. A single $GlnA_1$ protomer is composed of 15 β-strands and 15 α-helices and is
223 split in into a larger C-domain and an N-domain by helix α3. The dodecameric arrangement is
224 achieved through two distinct interfaces, the hexamer interfaces and inter-hexamer interfaces.

225 Hexamer interfaces are situated between subunits within each ring, while inter-hexamer interfaces
226 occur between subunits derived from adjacent rings (Fig. 4A, B, C). The structures are highly similar
227 to Gram-positive bacterial GS structures (PDB: 4lnn, Murray et al., 2013),with root mean squared
228 deviations (rmsds) of 0.5–1.0 Å.

229 A closer inspection of the density reveals the density for the bound 2-OG at an allosteric site localized
230 at the interface between two $GlnA_1$ protomers in vicinity of the $GlnA_1$ catalytic site (Fig. 4B, D).
231 Several residues are contributing to its binding. R172' and S189' coordinate the γ-Carboxy-group.
232 Additionally, two tightly bound water molecules are detectable in the binding site. One is interacting
233 with the γ-Carboxy group while being stabilized by another water that is coordinated by S38 and R26.
234 Latter arginine is coordinating the α-Keto-group and, together with R87 and R173', the α-Carboxy
235 group of 2-OG (Fig. 4B). Notably, F24 stabilizes the 2-OG via stacking with its phenyl ring. This binding
236 contribution from two $GlnA_1$ protomers at the intersubunit junction enhances activation by boosting
237 readiness and the rate of full complex assembly. It operates akin to molecular glue that facilitate the
238 observed cooperative assembly.

239 A comparison with the substrate-bound $GlnA_1$ structure (PDB: 8tfk, Schumacher et al. 2023) revealed
240 that the catalytically important residues in *M. mazei* are the aspartic acid (D57) that abstracts the
241 proton from ammonium and the catalytic glutamic acid, Glu307. The active site of *M. mazei* $GlnA_1$ is
242 formed at the interface between two subunits in the hexamer and formed by five key catalytic
243 elements surrounding the active site: the E flap (residues 303–310), the Y loop (residues 369–377),
244 the N loop (residues 235–247), the Y^* loop (residues 152–161) and the D50′ loop (residues 56-71).
245 The latter one is the only one that originates from adjacent neighboring protomer (Fig 5C, E).

246 Superposition of our structure with the apo- *M. mazei* X-ray structure (PDB: 8tfb, Schumacher et al.,
247 2023) reveals that 2-OG binding also triggers further movements that lead to structural changes in
248 the substrate binding pocket (Fig. 5A, B, D). R87' and its loop undergo a dramatic flip to coordinate 2-
249 OG and D170 of helix α3 (residues 167-181) (Fig. 5A). This, combined with the action of other
250 coordinating residues, initiates a motion that is propagated through the entire protein. Notably, helix
251 α3 shifts forward, causing F184 to flip over and facilitate a T-shaped aromatic interaction with F202.
252 The resulting pull on F202 causes F204 to flip, allowing π-stacking with the purine moiety of ATP (Fig.
253 5B). This series of structural changes primes the active site for ATP binding by already adopting the
254 side chain conformations that are observed in analogue (Met-Sox-P-ADP)-bound structure (transition
255 state) (PDB: 8tfk, Schumacher et al., 2023), thus facilitating nucleotide binding (Fig. 5C, E).

256 Additionally, the D50' loop adopts a position similar to the transition state in a catalytic competent
257 conformation. This involved a remodeling of the loop, leading to the positioning of key catalytic

258 residues in a catalytic competent configuration. Compared to the apo structure (Schumacher et al.,
259 2023), R66 flips out of the catalytic pocket, now accommodating R319 which participates in
260 phosphoryl transfer catalysis (Fig. 5D). In addition, Asp 57' moves deeper into the binding site,
261 facilitating the proton abstraction of NH_4^+ and preparing for its attack on the phosphorylated
262 glutamate. Similar to the ATP/ADP binding site, these catalytic elements are primed to ideally
263 stabilize the tetrahedral transition state. This is illustrated by the superposition of the inhibitor-
264 bound, transition-state locked structure (Schumacher et al., 2023) (Fig. 5C, E).

265 **Figure 5**

266

267 *Feedback inhibition by glutamine does not affect the dodecameric* M. mazei *$GlnA_1$ structure*

268 For bacteria it is known, that GS can be feedback inhibited. Very recently, the first feedback inhibition
269 of an archaeal GS by glutamine has been reported for *Methermicoccus shengliensis* GS (Müller et al.,
270 2023). The specific arginine residue identified to be relevant for the feedback inhibition is R66.
271 Consequently, we generated the respective *M. mazei* $GlnA_1$ mutant protein changing the conserved
272 arginine to alanine (R66A) (see also Fig. 5D, E) and compared the purified strep-tagged mutant
273 protein with the wildtype (wt) protein. In the presence of 12.5 mM 2-OG, the mutant protein showed
274 the same specific activity as obtained for the wt. However, when supplementing 5 mM glutamine,
275 exclusively the wt was strongly feedback inhibited, whereas the R66A mutant protein was not
276 significantly affected (Fig. 6A). In *B. subtilis*, R62 is responsible for feedback inhibition. The
277 superposition of the apo-BsGS structure (PDB: 4lnn, Murray et al., 2013) with our 2-OG-bound $GlnA_1$
278 reveals a similar positioning of the respective *M. mazei* R66 (Fig. 6B) indicating a similar mechanism.
279 Moreover, we can rule out an effect on the oligomeric structure of $GlnA_1$ by MP analysis, clearly
280 showing that glutamine does not induce disassembly of the dodecameric wt $GlnA_1$ (Fig. 6C). Instead,
281 this effect can be explained with the role of R66 being an important residue to bind to glutamine in
282 the product state of the enzyme.

283 **Figure 6**

284

285 **DISCUSSION**

286 *2-OG is crucially required for M. mazei GS assembly to an active dodecamer and induces the*
287 *conformational state towards an active open state*

288 In *M. mazei* increased 2-OG concentrations act as central N starvation signal (Ehlers et al., 2005).
289 Here we demonstrated the importance of 2-OG as the major regulator of *M. mazei* $GlnA_1$ activity by

290 using independent methods, MP and cryo-EM, to detect and structurally characterize single
291 complexes with high resolution and quantify the different oligomeric complexes. We have found
292 mono- and dimeric $GlnA_1$ (apo $GlnA_1$) to be inactive and crucially require 2-OG to form an active
293 dodecameric complex. Moreover, this dodecameric conformation is the only active state of $GlnA_1$. In
294 the first step, 2-OG assembles the dodecamer by binding at the interface of two subunits (Fig. 4B)
295 and functions as a molecular glue between neighbouring subunits. The assembly upon 2-OG addition
296 observed using MP appears to be cooperative, fast and without any detectable intermediate states
297 (Fig. 1B, C). Only immediately after thawing a frozen purified $GlnA_1$ preparation and in case that no
298 additional SEC was performed prior to MP analysis, samples showed additional octameric complexes
299 in MP with low abundancy (suppl. Fig. S4). However, octameric complexes were never observed in
300 cryo-EM or detected by SEC analysis of frozen purified $GlnA_1$ samples. Consequently, octamers are
301 most likely broken or disassembled $GlnA_1$-dodecamers or dead-ends in assembly with no
302 physiological function, rather than an incomplete dodecamer during assembly. Thus, our findings are
303 contrary to the assembly model proposed by Schuhmacher et al. (Schumacher et al., 2023).

304 As a second step of activation, the allosteric binding of 2-OG causes a series of conformational
305 changes in $GlnA_1$ protomers, which prime the active site for the transition state and hence catalysis
306 of the enzyme. This conformational change of the ATP-binding pocket of the dodecameric $GlnA_1$
307 upon 2-OG binding goes hand in hand with the observed increased activity at higher 2-OG
308 concentrations (Fig. 1). Comparing our 2-OG-bound $GlnA_1$ dodecameric structure and the
309 dodecameric *M. mazei* $GlnA_1$ transition state (PDB: 8tfk) and apo structures (PDB: 8ftb) reported by
310 Schumacher et al. (Schumacher et al., 2023), clearly demonstrates that 2-OG transfers $GlnA_1$ into its
311 open transition state conformation (Fig. 5). The conformation of our 2-OG-bound dodecamer
312 resembled the transition state conformation (ADP-Met-Sox-bound complex) reported by Schumacher
313 et al., even though in our case no ATP was added (Fig. 5E). A reconfiguration of the active site upon
314 2-OG-binding has also been reported for GS in *Methanothermococcus thermolithotrophicus* (Müller
315 et al., 2024). In this report, which does not delineate dodecamer assembly at all, it was demonstrated
316 that binding of 2-OG in one protomer-protomer interface of a dodecameric GS causes a cooperative
317 domino effect in the hexameric ring of *M. thermolithotrophicus* GS (Müller et al., 2024). A 2-OG
318 bound protomer undergoes a conformational change and thereby induces the same shift in its
319 neighbouring protomer (Müller et al., 2024). This is comparable to our observed cooperativity of *M.*
320 *mazei* dodecamer assembly at low 2-OG concentrations (K_D = 0.75 mM, percentage of dodecamer).
321 On the other hand, *M. mazei* $GlnA_1$ reaches maximal activity only at much higher 2-OG
322 concentrations and likely requires a fully 2-OG-occupied dodecamer for maximal activity. The here
323 obtained high activities by 2-OG saturation (up to 9 U/mg) in comparison with previously described
324 *M. mazei* $GlnA_1$ activities in the absence of 2-OG in the significantly lower range (mU/mg) (Gutt et

325 al., 2021; Schumacher et al., 2023) support our conclusion that 2-OG is substantial for the $GlnA_1$
326 active state.

327 *$GlnA_1$ activity is further regulated by feedback inhibition, small proteins and possibly filament*
328 *formation*

329 *M. mazei* $GlnA_1$ belongs to the group of Iα-type GS, which are known to be feedback inhibited. We
330 confirmed a strong feedback inhibition by a genetic approach and found R66 to be the key residue
331 for this inhibition (Fig. 6) as suggested in Müller et al. 2024. The mechanism of feedback inhibition
332 has been described in detail for *B. subtilis* GS (Murray et al., 2013). There, R62 plays the central role
333 by binding glutamine and inducing a well ordered inactive structure at the substrate-binding pocket
334 upon glutamine-binding (Murray et al., 2013). The homologous *M. mazei* R66 likely conveys a similar
335 way of inhibition to *B. subtilis* GS (Fig. 6B, alignment in suppl. Fig. S5).

336 Further regulations by the two small proteins sP26 and the PII-like protein $GlnK_1$ have previously
337 been reported for *M. mazei* (Ehlers et al., 2005; Gutt et al., 2021; Schumacher et al., 2023). However,
338 in the present study neither an interaction with $GlnK_1$, nor $GlnK_1$ effects on $GlnA_1$ complex formation
339 analysed by MP, nor an effect of $GlnK_1$ on $GlnA_1$ activity was detectable under the conditions used at
340 varying 2-OG concentrations (0.1 to 12.5 mM) and ratios of $GlnK_1$ to $GlnA_1$ (20:1, 2:1, 2:10) (Fig. 2).
341 Moreover, the addition of $GlnK_1$ did not result in a change of the K_D for 2-OG for the dodecamer
342 $GlnA_1$ assembly (Fig. 2D). In previous reports, $GlnK_1$ was shown to interact with $GlnA_1$ in vivo after a
343 nitrogen upshift by pull-down approaches (Ehlers et al., 2005), pointing towards an inhibitory
344 function of $GlnK_1$ under shifting conditions from N limitation to N sufficiency. Similarly, we could not
345 determine a cryo-EM structure including sP26 despite adding large excess of the small protein either
346 obtained by co-expression or by addition of a synthetic peptide. Because these attempts were
347 unsuccessful, we speculate that yet unknown cellular factor(s) might be required for an interaction of
348 $GlnA_1$ with both small proteins, $GlnK_1$ and sP26, which however is difficult to simulate under in vitro
349 conditions with purified proteins. Taken this into account, we speculate about a potential function of
350 the two small proteins beyond $GlnA_1$ inactivation or activation. Since the $GlnA_1$ reaction is coupled to
351 the GOGAT reaction (GS/GOGAT system) and the products of the two reactions replenish the
352 substrates for one other, it is tempting to speculate that $GlnA_1$ and GOGAT experience metabolic
353 coupling by sP26 and/or $GlnK_1$ e.g. by being involved in recruiting or separating GOGAT from $GlnA_1$.

354 Finally, higher oligomeric states of GS enzymes have been known for a long time for organisms like
355 yeast and *E. coli* (He et al., 2009; Huang et al., 2022; Petrovska et al., 2014; Valentine et al., 1968).
356 Interestingly, dependent on the ice thickness and on higher concentrated areas of the grids, we could
357 also observe filament-like structures of *M. mazei* $GlnA_1$ in cryo-EM and resolved their structure at a
358 resolution of 6.9 Å (suppl. Fig. S6). Such $GlnA_1$ filaments are also detectable in the cryo-EM images of

359 Schumacher et al. 2023 but were not reported. Their interface is much alike the previously reported
360 *E.Coli* GS filament structures (Huang et al., 2022). The physiological relevance of filamentation in *M.*
361 *mazei* however remains unresolved and raises the question, whether an additional rapid modulation
362 of $GlnA_1$ activity through higher oligomeric states exists, as described e.g. for yeast GS most
363 depending on stress conditions (Petrovska et al., 2014).

364 M. mazei *$GlnA_1$ shows unique properties*

365 Overall, we have confirmed 2-OG to be the central activator of $GlnA_1$ in *M. mazei,* which assembles
366 the active dodecamer and induces a conformational switch towards an active open state. Though 2-
367 OG has previously been reported as an on-switch for (methano)archaeal GS activity (Ehlers et al.,
368 2005; Müller et al., 2024; Pedro-Roig et al., 2013), the 2-OG-triggered assembly is novel and
369 described exclusively for *M. mazei* $GlnA_1$. In this respect, the way of GS regulation in *M. mazei* is
370 unique across all prokaryotic GS studied so far. Neither in cyanobacteria, enterobacteria or *Bacillus* is
371 2-OG a direct activator, nor is complex (dis-)assembly a mode of regulating GS activity in any other of
372 these model organisms. This is further supported by the absence of up to three of those four
373 arginines - coordinating 2-OG in *M. mazei* $GlnA_1$ - in these organisms (suppl. Fig. S5). The
374 cyanobacterial, enterobacterial and gram positive GS are present in the cell as active dodecamers
375 (Almassy et al., 1986; Bolay et al., 2018; Deuel et al., 1970). However, these dodecamers are
376 inactivated upon sudden N sufficiency through very different mechanisms: *Synechocystis* GS is
377 blocked by small proteins (inhibitory factors), the enterobacterial GS experiences gradual
378 adenylylation of subunits which abolishes the enzyme activity and *B. subtilis* GS is feedback inhibited
379 by glutamine and further inhibited by binding of the transcription factor GlnR (Almassy et al., 1986;
380 Bolay et al., 2018; Klähn et al., 2018, 2015; Stadtman, 2001; Travis et al., 2022b) (see Fig. 7).

381 The direct 2-OG activation and glutamine feedback inhibition of *M. mazei* GS are two fast, reversible
382 and very direct ways of reacting towards the changing N status of the cell. We propose that the
383 direct activation through 2-OG without any required additional protein as it is the case for all other
384 regulations, is a more simple and direct regulation of GS. Due to the evolutionary placement of
385 methanoarchaea and haloarchaea, where a direct 2-OG regulation has been found exclusively, this
386 may represent an ancient regulation.

387

388

389

390 **MATERIALS AND METHODS**

391 *Strains and plasmids*

392 For heterologous expression and purification of Strep-tagged $GlnA_1$ (MM_0964), the plasmid
393 pRS1841 was constructed. The $glnA_1$-sequence along with the sP26-sequence (including start-codon:
394 ATG) were codon-optimized for *Escherichia coli* expression and commercially synthesized by Eurofins
395 Genomics on the same plasmid (pRS1728) (Ebersberg, Germany). Polymerase chain reaction (PCR)
396 was performed using pRS1728 as template and the primers (Eurofins Genomics, Ebersberg,
397 Germany) GlnAopt_NdeI_for (5'TTTCATATGGTTCAGATGAAAAAATG3') and GlnA1opt_BamHI_rev
398 (5'TTTGGATCCTTACAGCATGCTCAGATAACGG3'). The resulting $GlnA_1$_opt PCR-product and vector
399 pRS375 were restricted with NdeI and BamHI (NEB, Schwalbach, Germany); the resulting pRS375
400 vector fragment and the $GlnA_1$ fragment were ligated resulting in pRS1841. For heterologous
401 expression of Strep-$GlnA_1$, pRS1841 was transformed in *E. coli* BL21 (DE3) cells (Thermo Fisher
402 Scientific, Waltham, Massachusetts) following the method of Inoue (Inoue et al., 1990). For
403 generating the Arg66Ala-mutant, a site-directed mutagenesis was performed. pRS1841 was PCR-
404 amplified using primers sdm_GlnA_R66A_for (5'ATTGAAGAAAGCGATATGAAACTGGCGC3') and
405 sdm_GlnA_R66A_rev (5'**CGC**GGTAAAGCCCTGAATGCTGCTACC3') by Phusion High-Fidelity polymerase
406 (Thermo Fisher Scientific, Waltham, Massachusetts) followed by religation resulting in plasmid
407 pRS1951. For heterologous expression, pRS1951 was transformed into *E. coli* BL21 (DE3).

408 In order to co-express sP26 along with Strep-$GlnA_1$, the construct pRS1863 was generated. pRS1728
409 with the codon-optimized sP26-sequence and pET21a (Novagen, Darmstadt, Germany) were
410 restricted with NdeI and NotI and the resulting untagged sP26_opt was ligated into the pET21a
411 backbone yielding pRS1863. pRS1863 was co-transformed with pRS1841 into *E. coli* BL21 (DE3) cells
412 (Thermo Fisher Scientific, Waltham, Massachusetts) selecting for both Kanamycin (pRS1841 derived)
413 and Ampicillin (pRS1863 derived) resistance.

414 The plasmid pRS1672 was constructed for producing untagged $GlnK_1$. The $GlnK_1$ gene was PCR-
415 amplified using primers GlnK1_MM0732.for (5'ATGGTTGGCTATGAAATACGTAATTG3') and
416 GlnK1_MM0732.rev (5'TCAAATTGCCTCAGGTCCG3') and cloned into pETSUMO by using the
417 Champion™ pET SUMO Expression System (Thermo Fisher Scientific, Waltham, Massachusetts)
418 according to the manufacturer's protocol. pRS1672 was then transformed into *E. coli* DH5α and BL21
419 (DE3) pRIL (suppl. Tab. S1).

420 *Heterologous expression and protein purification: Strep-$GlnA_1$ and $GlnK_1$*

421 Heterologous expression of Strep-$GlnA_1$-variants (pRS1841 and pRS1951) and Strep-$GlnA_1$-sP26-
422 coexpression (pRS1841 + pRS1863) were performed in 1 l Luria Bertani medium (LB,

423 Carl Roth GmbH + Co. KG, Karlsruhe, Germany). *E. coli* BL21 (DE3) containing pRS1841, pRS1841 and
424 pRS1863 or pRS1951 was grown to an optical turbidity at 600 nm (T_{600}) of 0.6 - 0.8, induced with 25
425 µM isopropylβ-d-1-thiogalactopyranoside (IPTG, Carl Roth GmbH + Co. KG, Karlsruhe, Germany) and
426 further incubated over night at 18 °C and 120 rpm. The cells were harvested (6,371 x g, 20 min, 4 °C)
427 and resuspended in 6 ml W-buffer (100 mM TRIS/HCl, 150 mM NaCl, 2.5 mM EDTA, (chemicals from
428 Carl Roth GmbH + Co. KG, Karlsruhe, Germany), 12.5 mM 2-oxoglutarate (2-OG, Sigma-Aldrich, St.
429 Louis, Missouri), pH 8.0). After the addition of DNase I (Sigma-Aldrich, St. Louis, Missouri), cell
430 disruption was performed twice using a French Pressure Cell at 4.135 x 10^6 N/m^2 (*Sim-Aminco*
431 *Spectronic Instruments*, Dallas, Texas) followed by centrifugation of the cell lysate for (30 min (13,804
432 x g, 4 °C). The supernatant was incubated with 1 ml equilibrated (W-buffer) Strep-Tactin sepharose
433 matrix (IBA, Gottingen, Germany) at 4°C for 1 h at 20 rpm. Strep-tagged $GlnA_1$ was eluted from the
434 gravity flow column by adding E-buffer (W-buffer + 2.5 mM desthiobiotine (IBA, Gottingen,
435 Germany)). Strep-$GlnA_1$ was always purified and stored in the presence of 12.5 mM 2-OG, either in E-
436 buffer or 50 mM HEPES, pH 7.0 at 4 °C for a few days or with 5 % glycerol at -80 °C (chemicals from
437 Carl Roth GmbH + Co. KG, Karlsruhe, Germany).

438 His_6-SUMO-$GlnK_1$ was expressed similarly using *E. coli* BL21 (DE3) pRIL + pRS1672. Expression was
439 induced with 100 µM IPTG, incubated at 37 °C, 180 rpm for 2 h and harvested. The pellet was
440 resuspended in phosphate buffer (50 mM phosphate, 300 mM NaCl, pH 8 (chemicals from
441 Carl Roth GmbH + Co. KG, Karlsruhe, Germany)) and the cell extract was prepared as described
442 above. His-tag-affinity chromatography-purifcation was performed with a Ni-NTA agarose (Qiagen,
443 Hilden, Germany) gravity flow column, the protein was purified by stepwise-elution with 100 and 250
444 mM imidazole (SERVA, Heidelberg, Deutschland) in phosphate buffer. SUMO-protease (Thermo
445 Fisher Scientific, Waltham, Massachusetts) was used according to the manufacturer's protocol to
446 cleave the His_6-SUMO-$GlnK_1$ and obtain untagged $GlnK_1$ by passing through the Ni-NTA-column after
447 the cleavage. Elution fractions of protein purifications were analyzed on 12 % SDS-PAGE gels and the
448 protein concentrations were determined by Bradford (Bio-Rad Laboratories, Hercules, California) or
449 Qubit protein assay (Thermo Fisher Sceintific, Waltham, Massachusetts).

450 *Determination of glutamine synthetase activity*

451 The glutamine synthetase activity was determined by performing a coupled optical assay (Shapiro
452 and Stadtman, 1970). The assay was performed as described in Gutt et al. 2021 with modifications.
453 Modifcations included the use of 50 mM HEPES, the adjustment of ATP-pH to 7.0 and the use of 5
454 mM glutamine (Sigma-Aldrich, St. Louis, Missouri) in some assays. The assays were performed with
455 four technical replicates per condition including two concentrations of GnA_1 (2 x 10 µg and 2 x 20 µg
456 of Strep-$GlnA_1$). Strep-$GlnA_1$ was stored in E-buffer or 50 mM HEPES containing 12.5 mM 2-OG which

457 was dialysed against 50 mM HEPES pH 7 using Amicon® Ultra catridges with 30 kDa filters
458 (MilliporeSigma, Burlington, Massachusetts) for the enzyme assays in the absence of 2-OG.

459 *Mass photometry*

460 The molecular weight of protein complexes was analysed by mass photometry (MP) using a Refeyn
461 twoMP mass photometer with the AcquireMP software (Refeyn Ltd., Oxford, UK). All measurements
462 were performed in 50 mM HEPES, 150 mM NaCl pH 7.0 (MP-buffer, chemicals from
463 Carl Roth GmbH + Co. KG, Karlsruhe, Germany) on 1.5 H, 24 x 60 mm microscope coverslips with
464 Culture Well Reusable Gaskets (GRACE BIO-LABS, Bend, Oregon). Strep-$GlnA_1$ and untagged $GlnK_1$
465 were prepared as described above. Prior to MP experiments, a size exclusion chromatography (SEC)
466 was performed with $GlnA_1$ in the presence of 12.5 mM 2-OG on a Superose™ 6 Increase 10/300 GL
467 column (Cytiva, Marlborough, Massachusetts) with a flow rate of 0.5 ml/min. Only the dodecameric
468 fraction was used for MP experiments and dialysed against MP buffer using Amicon® Ultra catridges
469 with 30 kDa filters (MilliporeSigma, Burlington, Massachusetts) beforehand. The Gel Filtration HMW
470 Calibration Kit (Cytiva, Marlborough, Massachusetts) was used as a standard in SEC. 75 – 200 nM
471 monomeric Strep-$GlnA_1$ were used in the MP measurements, $GlnK_1$ was added accordingly in the
472 desired ratio calculated based on monomers. The analysis of the acquired data was performed with
473 the DiscoverMP software by applying a pre-measured standard (Refeyn Ltd., Oxford, UK). Counts
474 were visualized in mass histograms as relative counts, which were calculated for the Gaussian fits of
475 the measured peaks. For the determination of K_D-values and creating sigmoidal fitted curves, RStudio
476 (RStudio Team (2020). RStudio: Integrated Development for R. RStudio, PBC, Boston, MA URL) was
477 used.

478 *Cryo-electron sample preparation and Data collection:*

479 Purified GS at a concentration of 1.5 mg/mL was rapidly applied to glow-discharged Quantifoil grids,
480 blotted with force 4 for 3.5 s, and vitrified by directly plunging in liquid ethane (cooled by liquid
481 nitrogen) using Vitrobot Mark IV (Thermo Fisher Scientific, Waltham, Massachusetts) at 100%
482 humidity and 4 °C. To overcome prefererred orientation bias, 0.7 mM CHAPSO was added to prevent
483 water-air interface interactions, consequently the concentration of the protein was increased to
484 6mg/ml. We added purified commercially synthesized sP26 (Davids Biotechnologie, Regensburg,
485 Germany) to all samples, but the peptide did not stably bind under the observed conditions. Data
486 was acquired with EPU in EER-format on an FEI Titan Krios G4 (Cryo-EM Platform, Helmholtz Munich)
487 equipped with a Falcon IVi detector (Thermo Fisher Scientific, Waltham, Massachusetts) with a total
488 electron dose of ~55 electrons per $Å^2$ and a pixel size of 0.76 Å. Micrographs were recorded in a
489 defocus range of -0.25 to -2.0 µm. For details see suppl. Table S2.

Cryo EM - Image processing, classification and refinement

All data was processed using Cryosparc (Punjani et al., 2017). Micrographs were processed on the fly (motion correction, CTF estimation). Using blob picker, 878,308 particles were picked, 2D-classified and used for ab initio reconstruction. Iterative rounds of ab initio and heterogenous refinement were used to clean the particle stacks. The final refinements yielded models with an estimated resolution of 2.39 Å sets at the 0.143 cutoff (suppl. Fig. S3).

An initial model was generated from the protein sequences using alphaFold (Jumper et al., 2021), and thereupon fitted as rigid bodies into the density using UCSF Chimera (Pettersen et al., 2021). The model was manually rebuilt using *Coot* (Emsley et al., 2010). The final model was subjected to real-space refinements in PHENIX (Liebschner et al., 2019). Illustrations of the models were prepared using UCSF ChimeraX (Pettersen et al., 2021). The structure is accessible under PDB: 8s59. For details see suppl. Table S2.

Acknowledgements.

We thank the members of our laboratories for useful discussions on the experiments, as well as Claudia Kiessling for technical assistance. This work was supported by the German Research Council (DFG) priority program (SPP) 2002 'Small proteins in Prokaryotes, an unexplored world' [Schm1052/20-2]. We acknowledge the contribution of the CryoEM Facility of the Philipps University of Marburg. J.M.S. acknowledges the DFG for an Emmy Noether grant (SCHU 3364/1-1) cofunded by the European Union (ERC, TwoCO2One, 101075992). Views and opinions expressed are, however, those of the author(s) only and do not necessarily reflect those of the European Union or the European Research Council. Neither the European Union nor the granting authority can be held responsible for them. We thank Sandra Schuller for useful discussions and help in preparing manuscript figures. GKAH was supported by the Max Planck Society.

516

517 REFERENCES

518 Almassy, R.J., Janson, C.A., Hamlin, R., Xuong, N.-H., Eisenberg, D., 1986. Novel subunit—subunit
519 interactions in the structure of glutamine synthetase. Nature 323, 304–309.
520 https://doi.org/10.1038/323304a0

521 Bolay, P., Muro-Pastor, M.I., Florencio, F.J., Klähn, S., 2018. The Distinctive Regulation of
522 Cyanobacterial Glutamine Synthetase. Life 8, 52. https://doi.org/10.3390/life8040052

523 Brown, J.R., Masuchi, Y., Robb, F.T., Doolittlel, W.F., 1994. Evolutionary relationships of bacterial and
524 archaeal glutamine synthetase genes. J. Mol. Evol. 38, 566–576.
525 https://doi.org/10.1007/BF00175876

526 Cohen-Kupiec, R., Marx, C.J., Leigh, J.A., 1999. Function and regulation of glnA in the methanogenic
527 archaeon Methanococcus maripaludis. J. Bacteriol. 181, 256–261.
528 https://doi.org/10.1128/JB.181.1.256-261.1999

529 Deuel, T.F., Ginsburg, A., Yeh, J., Shelton, E., Stadtman, E.R., 1970. Bacillus subtilis glutamine
530 synthetase. Purification and physical characterization. J. Biol. Chem. 245, 5195–5205.

531 Dos Santos Moreira, C.D., Ramos, M.J.R.N., Fernandes, P.M.A.A., 2019. Glutamine synthetase
532 structure-catalysis relationship—Recent advances and applications. WIREs Comput. Mol. Sci. 9,
533 e1399. https://doi.org/10.1002/wcms.1399

534 Ehlers, C., Weidenbach, K., Veit, K., Forchhammer, K., Schmitz, R.A., 2005. Unique mechanistic
535 features of post-translational regulation of glutamine synthetase activity in *Methanosarcina mazei*
536 strain Gö1 in response to nitrogen availability: Regulation of glutamine synthetase activity in *M.*
537 *mazei*. Mol. Microbiol. 55, 1841–1854. https://doi.org/10.1111/j.1365-2958.2005.04511.x

538 Emsley, P., Lohkamp, B., Scott, W.G., Cowtan, K., 2010. Features and development of *Coot*. Acta
539 Crystallogr. D Biol. Crystallogr. 66, 486–501. https://doi.org/10.1107/S0907444910007493

540 Fedorova, K., Kayumov, A., Woyda, K., Ilinskaja, O., Forchhammer, K., 2013. Transcription factor TnrA
541 inhibits the biosynthetic activity of glutamine synthetase in Bacillus subtilis. FEBS Lett. 587, 1293–
542 1298. https://doi.org/10.1016/j.febslet.2013.03.015

543 Fisher, S.H., 1999. Regulation of nitrogen metabolism in Bacillus subtilis: vive la différence! Mol.
544 Microbiol. 32, 223–232. https://doi.org/10.1046/j.1365-2958.1999.01333.x

545 Fisher, S.H., Wray, L.V., 2008. Bacillus subtilis glutamine synthetase regulates its own synthesis by
546 acting as a chaperone to stabilize GlnR-DNA complexes. Proc. Natl. Acad. Sci. U. S. A. 105, 1014–
547 1019. https://doi.org/10.1073/pnas.0709949105

548 Forchhammer, K., 1999. The PII Protein in Synechococcus PCC 7942 Senses and Signals 2-
549 Oxoglutarate Under ATP-Replete Conditions, in: Peschek, G.A., Löffelhardt, W., Schmetterer, G.
550 (Eds.), The Phototrophic Prokaryotes. Springer US, Boston, MA, pp. 549–553.
551 https://doi.org/10.1007/978-1-4615-4827-0_63

García-Domínguez, M., Reyes, J.C., Florencio, F.J., 1999. Glutamine synthetase inactivation by protein–protein interaction. Proc. Natl. Acad. Sci. 96, 7161–7166. https://doi.org/10.1073/pnas.96.13.7161

Gunka, K., Commichau, F.M., 2012. Control of glutamate homeostasis in Bacillus subtilis: a complex interplay between ammonium assimilation, glutamate biosynthesis and degradation. Mol. Microbiol. 85, 213–224. https://doi.org/10.1111/j.1365-2958.2012.08105.x

Gutt, M., Jordan, B., Weidenbach, K., Gudzuhn, M., Kiessling, C., Cassidy, L., Helbig, A., Tholey, A., Pyper, D.J., Kubatova, N., Schwalbe, H., Schmitz, R.A., 2021. High complexity of Glutamine synthetase regulation in Methanosarcina mazei: Small protein 26 interacts and enhances glutamine synthetase activity. FEBS J. n/a. https://doi.org/10.1111/febs.15799

Hanahan, D., 1983. Studies on transformation of Escherichia coli with plasmids. J. Mol. Biol. 166, 557–580. https://doi.org/10.1016/s0022-2836(83)80284-8

Hauf, K., Kayumov, A., Gloge, F., Forchhammer, K., 2016. The Molecular Basis of TnrA Control by Glutamine Synthetase in Bacillus subtilis*. J. Biol. Chem. 291, 3483–3495. https://doi.org/10.1074/jbc.M115.680991

He, Y.-X., Gui, L., Liu, Y.-Z., Du, Y., Zhou, Y., Li, P., Zhou, C.-Z., 2009. Crystal structure of Saccharomyces cerevisiae glutamine synthetase Gln1 suggests a nanotube-like supramolecular assembly. Proteins Struct. Funct. Bioinforma. 76, 249–254. https://doi.org/10.1002/prot.22403

Herrero, A., Muro-Pastor, A.M., Flores, E., 2001. Nitrogen Control in Cyanobacteria. J. Bacteriol. 183, 411–425. https://doi.org/10.1128/jb.183.2.411-425.2001

Ho, C.-M., Li, X., Lai, M., Terwilliger, T.C., Beck, J.R., Wohlschlegel, J., Goldberg, D.E., Fitzpatrick, A.W.P., Zhou, Z.H., 2020. Bottom-up structural proteomics: cryoEM of protein complexes enriched from the cellular milieu. Nat. Methods 17, 79–85. https://doi.org/10.1038/s41592-019-0637-y

Huang, P.-C., Chen, S.-K., Chiang, W.-H., Ho, M.-R., Wu, K.-P., 2022. Structural basis for the helical filament formation of Escherichia coli glutamine synthetase. Protein Sci. 31, e4304. https://doi.org/10.1002/pro.4304

Inoue, H., Nojima, H., Okayama, H., 1990. High efficiency transformation of Escherichia coli with plasmids. Gene 96, 23–28. https://doi.org/10.1016/0378-1119(90)90336-p

Jäger, D., Sharma, C.M., Thomsen, J., Ehlers, C., Vogel, J., Schmitz, R.A., 2009. Deep sequencing analysis of the Methanosarcina mazei Gö1 transcriptome in response to nitrogen availability. Proc. Natl. Acad. Sci. 106, 21878–21882. https://doi.org/10.1073/pnas.0909051106

Jiang, P., Peliska, J.A., Ninfa, A.J., 1998. Reconstitution of the signal-transduction bicyclic cascade responsible for the regulation of Ntr gene transcription in Escherichia coli. Biochemistry 37, 12795–12801. https://doi.org/10.1021/bi9802420

Joo, H.K., Park, Y.W., Jang, Y.Y., Lee, J.Y., 2018. Structural Analysis of Glutamine Synthetase from Helicobacter pylori. Sci. Rep. 8, 11657. https://doi.org/10.1038/s41598-018-30191-5

588 Jumper, J., Evans, R., Pritzel, A., Green, T., Figurnov, M., Ronneberger, O., Tunyasuvunakool, K.,
589 Bates, R., Žídek, A., Potapenko, A., Bridgland, A., Meyer, C., Kohl, S.A.A., Ballard, A.J., Cowie, A.,
590 Romera-Paredes, B., Nikolov, S., Jain, R., Adler, J., Back, T., Petersen, S., Reiman, D., Clancy, E.,
591 Zielinski, M., Steinegger, M., Pacholska, M., Berghammer, T., Bodenstein, S., Silver, D., Vinyals, O.,
592 Senior, A.W., Kavukcuoglu, K., Kohli, P., Hassabis, D., 2021. Highly accurate protein structure
593 prediction with AlphaFold. Nature 596, 583–589. https://doi.org/10.1038/s41586-021-03819-2

594 Klähn, S., Bolay, P., Wright, P.R., Atilho, R.M., Brewer, K.I., Hagemann, M., Breaker, R.R., Hess, W.R.,
595 2018. A glutamine riboswitch is a key element for the regulation of glutamine synthetase in
596 cyanobacteria. Nucleic Acids Res. https://doi.org/10.1093/nar/gky709

597 Klähn, S., Schaal, C., Georg, J., Baumgartner, D., Knippen, G., Hagemann, M., Muro-Pastor, A.M.,
598 Hess, W.R., 2015. The sRNA NsiR4 is involved in nitrogen assimilation control in cyanobacteria by
599 targeting glutamine synthetase inactivating factor IF7. Proc. Natl. Acad. Sci. 112.
600 https://doi.org/10.1073/pnas.1508412112

601 Legrain, C., Vissers, S., Dubois, E., Legrain, M., Wiame, J.-M., 1982. Regulation of Glutamine
602 Synthetase from Saccharomyces cerevisiae by Repression, Inactivation and Proteolysis. Eur. J.
603 Biochem. 123, 611–616. https://doi.org/10.1111/j.1432-1033.1982.tb06576.x

604 Liaw, S.H., Pan, C., Eisenberg, D., 1993. Feedback inhibition of fully unadenylylated glutamine
605 synthetase from Salmonella typhimurium by glycine, alanine, and serine. Proc. Natl. Acad. Sci. U. S. A.
606 90, 4996–5000. https://doi.org/10.1073/pnas.90.11.4996

607 Lie, T.J., Dodsworth, J.A., Nickle, D.C., Leigh, J.A., 2007. Diverse homologues of the archaeal repressor
608 NrpR function similarly in nitrogen regulation. FEMS Microbiol. Lett. 271, 281–288.
609 https://doi.org/10.1111/j.1574-6968.2007.00726.x

610 Liebschner, D., Afonine, P.V., Baker, M.L., Bunkóczi, G., Chen, V.B., Croll, T.I., Hintze, B., Hung, L.-W.,
611 Jain, S., McCoy, A.J., Moriarty, N.W., Oeffner, R.D., Poon, B.K., Prisant, M.G., Read, R.J., Richardson,
612 J.S., Richardson, D.C., Sammito, M.D., Sobolev, O.V., Stockwell, D.H., Terwilliger, T.C., Urzhumtsev,
613 A.G., Videau, L.L., Williams, C.J., Adams, P.D., 2019. Macromolecular structure determination using X-
614 rays, neutrons and electrons: recent developments in Phenix. Acta Crystallogr. Sect. Struct. Biol. 75,
615 861–877. https://doi.org/10.1107/S2059798319011471

616 Magasanik, B., 1993. The regulation of nitrogen utilization in enteric bacteria. J. Cell. Biochem. 51,
617 34–40. https://doi.org/10.1002/jcb.240510108

618 Masalkar, P.D., Roberts, D.M., 2015. Glutamine synthetase isoforms in nitrogen-fixing soybean
619 nodules: distinct oligomeric structures and thiol-based regulation. FEBS Lett. 589, 215–221.
620 https://doi.org/10.1016/j.febslet.2014.11.048

621 McMullan, G., Naydenova, K., Mihaylov, D., Yamashita, K., Peet, M.J., Wilson, H., Dickerson, J.L.,
622 Chen, S., Cannone, G., Lee, Y., Hutchings, K.A., Gittins, O., Sobhy, M.A., Wells, T., El-Gomati, M.M.,
623 Dalby, J., Meffert, M., Schulze-Briese, C., Henderson, R., Russo, C.J., 2023. Structure determination by
624 cryoEM at 100 keV. Proc. Natl. Acad. Sci. 120, e2312905120.
625 https://doi.org/10.1073/pnas.2312905120

626 Müller, M.-C., Lemaire, O.N., Kurth, J.M., Welte, C.U., Wagner, T., 2024. Differences in regulation
627 mechanisms of glutamine synthetases from methanogenic archaea unveiled by structural
628 investigations. Commun. Biol. 7, 1–14. https://doi.org/10.1038/s42003-023-05726-w

629 Müller, M.-C., Lemaire, O.N., Kurth, J.M., Welte, C.U., Wagner, T., 2023. Differences in the regulation
630 mechanisms of the glutamine synthetase from methanogenic archaea unveiled by structural
631 investigations. https://doi.org/10.1101/2023.04.07.535877

632 Murray, D.S., Chinnam, N., Tonthat, N.K., Whitfill, T., Wray, L.V., Fisher, S.H., Schumacher, M.A.,
633 2013. Structures of the Bacillus subtilis glutamine synthetase dodecamer reveal large intersubunit
634 catalytic conformational changes linked to a unique feedback inhibition mechanism. J. Biol. Chem.
635 288, 35801–35811. https://doi.org/10.1074/jbc.M113.519496

636 Nilsson, M.T., Krajewski, W.W., Yellagunda, S., Prabhumurthy, S., Chamarahally, G.N., Siddamadappa,
637 C., Srinivasa, B.R., Yahiaoui, S., Larhed, M., Karlén, A., Jones, T.A., Mowbray, S.L., 2009. Structural
638 basis for the inhibition of Mycobacterium tuberculosis glutamine synthetase by novel ATP-
639 competitive inhibitors. J. Mol. Biol. 393, 504–513. https://doi.org/10.1016/j.jmb.2009.08.028

640 Pedro-Roig, L., Camacho, M., Bonete, M.-J., 2013. Regulation of ammonium assimilation in Haloferax
641 mediterranei: interaction between glutamine synthetase and two GlnK proteins. Biochim. Biophys.
642 Acta 1834, 16–23. https://doi.org/10.1016/j.bbapap.2012.10.006

643 Petrovska, I., Nüske, E., Munder, M.C., Kulasegaran, G., Malinovska, L., Kroschwald, S., Richter, D.,
644 Fahmy, K., Gibson, K., Verbavatz, J.-M., Alberti, S., 2014. Filament formation by metabolic enzymes is
645 a specific adaptation to an advanced state of cellular starvation. eLife 3, e02409.
646 https://doi.org/10.7554/eLife.02409

647 Pettersen, E.F., Goddard, T.D., Huang, C.C., Meng, E.C., Couch, G.S., Croll, T.I., Morris, J.H., Ferrin,
648 T.E., 2021. UCSF ChimeraX: Structure visualization for researchers, educators, and developers.
649 Protein Sci. Publ. Protein Soc. 30, 70–82. https://doi.org/10.1002/pro.3943

650 Prasse, D., Schmitz, R.A., 2018. Small RNAs Involved in Regulation of Nitrogen Metabolism. Microbiol.
651 Spectr. 6. https://doi.org/10.1128/microbiolspec.RWR-0018-2018

652 Punjani, A., Rubinstein, J.L., Fleet, D.J., Brubaker, M.A., 2017. cryoSPARC: algorithms for rapid
653 unsupervised cryo-EM structure determination. Nat. Methods 14, 290–296.
654 https://doi.org/10.1038/nmeth.4169

655 Reitzer, L., 2003. Nitrogen Assimilation and Global Regulation in Escherichia coli. Annu. Rev.
656 Microbiol. 57, 155–176. https://doi.org/10.1146/annurev.micro.57.030502.090820

657 Schumacher, M.A., Salinas, R., Travis, B.A., Singh, R.R., Lent, N., 2023. M. mazei glutamine synthetase
658 and glutamine synthetase-GlnK1 structures reveal enzyme regulation by oligomer modulation. Nat.
659 Commun. 14, 7375. https://doi.org/10.1038/s41467-023-43243-w

660 Shapiro, B.M., Stadtman, E.R., 1970. [130] Glutamine synthetase (Escherichia coli), in: Methods in
661 Enzymology. Elsevier, pp. 910–922. https://doi.org/10.1016/0076-6879(71)17305-3

662 Stadtman, E.R., 2004. Regulation of Glutamine Synthetase Activity. EcoSal Plus 1,
663 10.1128/ecosalplus.3.6.1.6. https://doi.org/10.1128/ecosalplus.3.6.1.6

664 Stadtman, E.R., 2001. The story of glutamine synthetase regulation. J. Biol. Chem. 276, 44357–44364.
665 https://doi.org/10.1074/jbc.R100055200

666 Stadtman, E.R., 1990. [60] Discovery of glutamine synthetase cascade, in: Deutscher, M.P. (Ed.),
667 Methods in Enzymology, Guide to Protein Purification. Academic Press, pp. 793–809.
668 https://doi.org/10.1016/0076-6879(90)82062-7

669 Travis, B.A., Peck, J.V., Salinas, R., Dopkins, B., Lent, N., Nguyen, V.D., Borgnia, M.J., Brennan, R.G.,
670 Schumacher, M.A., 2022a. Molecular dissection of the glutamine synthetase-GlnR nitrogen
671 regulatory circuitry in Gram-positive bacteria. Nat. Commun. 13, 3793.
672 https://doi.org/10.1038/s41467-022-31573-0

673 Travis, B.A., Peck, J.V., Salinas, R., Dopkins, B., Lent, N., Nguyen, V.D., Borgnia, M.J., Brennan, R.G.,
674 Schumacher, M.A., 2022b. Molecular dissection of the glutamine synthetase-GlnR nitrogen
675 regulatory circuitry in Gram-positive bacteria. Nat. Commun. 13, 3793.
676 https://doi.org/10.1038/s41467-022-31573-0

677 Valentine, R.C., Shapiro, B.M., Stadtman, E.R., 1968. Regulation of glutamine synthetase. XII.
678 Electron microscopy of the enzyme from Escherichia coli. Biochemistry 7, 2143–2152.
679 https://doi.org/10.1021/bi00846a017

680 van Heeswijk, W.C., Westerhoff, H.V., Boogerd, F.C., 2013. Nitrogen Assimilation in Escherichia coli:
681 Putting Molecular Data into a Systems Perspective. Microbiol. Mol. Biol. Rev. 77, 628–695.
682 https://doi.org/10.1128/mmbr.00025-13

683 van Rooyen, J.M., Abratt, V.R., Belrhali, H., Sewell, T., 2011. Crystal structure of Type III glutamine
684 synthetase: surprising reversal of the inter-ring interface. Struct. Lond. Engl. 1993 19, 471–483.
685 https://doi.org/10.1016/j.str.2011.02.001

686 Veit, K., Ehlers, C., Schmitz, R.A., 2005. Effects of nitrogen and carbon sources on transcription of
687 soluble methyltransferases in Methanosarcina mazei strain Go1. J. Bacteriol. 187, 6147–6154.
688 https://doi.org/10.1128/JB.187.17.6147-6154.2005

689 Weidenbach, K., Ehlers, C., Kock, J., Ehrenreich, A., Schmitz, R.A., 2008. Insights into the NrpR regulon
690 in Methanosarcina mazei Gö1. Arch. Microbiol. 190, 319–332. https://doi.org/10.1007/s00203-008-
691 0369-3

692 Weidenbach, K., Ehlers, C., Kock, J., Schmitz, R.A., 2010. NrpRII mediates contacts between NrpRI and
693 general transcription factors in the archaeon Methanosarcina mazei Gö1. FEBS J. 277, 4398–4411.
694 https://doi.org/10.1111/j.1742-4658.2010.07821.x

695 Wisedchaisri, G., Dranow, D.M., Lie, T.J., Bonanno, J.B., Patskovsky, Y., Ozyurt, S.A., Sauder, J.M.,
696 Almo, S.C., Wasserman, S.R., Burley, S.K., Leigh, J.A., Gonen, T., 2010. Structural Underpinnings of
697 Nitrogen Regulation by the Prototypical Nitrogen-Responsive Transcriptional Factor NrpR. Structure
698 18, 1512–1521. https://doi.org/10.1016/j.str.2010.08.014

699 Woolfolk, C.A., Stadtman, E.R., 1967. Regulation of glutamine synthetase: III. Cumulative feedback
700 inhibition of glutamine synthetase from Escherichia coli. Arch. Biochem. Biophys. 118, 736–755.
701 https://doi.org/10.1016/0003-9861(67)90412-2

Yamashita, M., Almassy, R., Janson, C., Cascio, D., Eisenberg, D., 1989. Refined atomic model of glutamine synthetase at 3.5 Å resolution. J. Biol. Chem. 264, 17681–90. https://doi.org/10.2210/pdb2gls/pdb

706 **FIGURE LEGENDS**

707 **Figure 1**: **$GlnA_1$-dodecamer-assembly is induced by 2-OG without detectable oligomeric**
708 **intermediates**. Oligomerisation states of purified strep-tagged $GlnA_1$ were assessed in dependence of
709 2-OG by mass photometry as described in MM using a Refeyn twoMP mass photometer (Refeyn Ltd.,
710 Oxford, UK). Mass spectra are shown with relative counts (number of counts in relation to the total
711 counts) plotted against the molecular weight. **A**: 75 nM $GlnA_1$ were preincubated in the presence of
712 varying 2-OG concentrations (0 to 25 mM) for ten min at room temperature and kept on ice until
713 measurement. The percentage of dodecamer considering the total number of counts was plotted
714 against the 2-OG concentration. One out of two independent biological replicates with each three
715 technical replicates is shown exemplarily. The molecular masses shown above the peaks correspond
716 to a Gaussian fit of the respective peak (Gaussian fit not shown) and the K_D is indicated in green. **B**:
717 Exemplary mass spectra of $GlnA_1$ oligomers in the presence of 0.1 and 12.5 mM 2-OG. **C**: Mass
718 spectra of the three technical replicates (different green colors) of $GlnA_1$-oligomers at 0.39, 0.78 and
719 1.56 mM 2-OG, excluding the presence of intermediates. **D**: The specific activity of purified strep-
720 tagged $GlnA_1$ was determined as described in MM in the presence of varying 2-OG concentrations (0,
721 1.25, 5 and 12.5 mM). The standard deviation of four technical replicates is indicated for one out of
722 two biological replicates.

723

724 **Figure 2: $GlnA_1$-dodecamer-assembly and activity are not influenced by $GlnK_1$ under the conditions**
725 **tested**. Purified strep-tagged $GlnA_1$ and tag-less $GlnK_1$ were incubated in the absence or presence of
726 2-OG in varying concentrations for ten min at RT. Oligomerisation states were assessed by mass
727 photometry. Mass spectra are shown with relative counts (see Fig. 1). **A**: The obtained ratio of $GlnA_1$
728 dodecamer/dimer of three technical replicates are shown for varying ratios between $GlnA_1$ and $GlnK_1$
729 (20:1, 2:1, 2:10, ratios relating to monomers) in the absence of 2-OG. **B, C**: Exemplary mass spectra of
730 $GlnA_1$ incubated in the absence and presence of $GlnK_1$ (2:1) at 2-OG concentrations of 0 mM (B) and
731 12.5 mM (C). The molecular masses shown above the peaks correspond to a Gaussian fit of the
732 respective peak (Gaussian fit not shown). **D**: 200 nM monomeric $GlnA_1$ were preincubated with $GlnK_1$
733 (in a 2:1 ratio) in the presence of varying 2-OG concentrations (0.19 to 12.5 mM) for ten min at RT.
734 The percentage of $GlnA_1$ dodecamer considering the total number of counts was plotted against the
735 2-OG concentration. One biological replicate with three technical replicates was performed. The ratio
736 of $GlnA_1$ dodecamer/dimer was plotted against the 2-OG concentration and the KD is indicated in
737 green (●, - $GlnK_1$) and yellow (●, + $GlnK_1$). **E**: The specific activity of purified strep-tagged $GlnA_1$ in the
738 absence and presence of $GlnK_1$ (ratio 2:1) was determined as described in MM in the presence of

739 varying 2-OG concentrations (0, 0.78, 6.25 and 12.5 mM). The standard deviations of four technical
740 replicates of one biological replicate are indicated.
741
742
743 **Figure 3: Structure of *M. Mazei* $GlnA_1$ with 2-OG. A**: Three-dimensional segmented cryo-EM density
744 of the dodecameric complex colored by subunits. **B**: Corresponding views of the $GlnA_1$ atomic model
745 in cartoon representation.

746
747 **Figure 4: Dimeric Interface and 2-OG binding site of dodecameric $GlnA_1$. A**: Surface representation
748 of the *M. mazei* $GlnA_1$ 2-OG dodecamer with three $GlnA_1$ protomers fitted in cartoon representation
749 into the dodecamer as vertical (blue and ochre) and horizontal (blue and green) dimers. **B**: Horizontal
750 dimers and close-up of 2-OG binding site. Important residues are shown as atomic stick
751 representation, primed labels indicate neighboring protomer. 2-OG and water molecules important
752 for ligand binding fitted into density are shown in grey. Dotted lines represent polar interactions
753 between 2-OG, waters and residues. **C** Vertical dimers and close-up of dimerization site. C-terminal
754 helices H14/15 and H14'/ H15' of two neighboring protomers lead to tight interaction, mediated by
755 hydrophobic and polar interactions. **D**: Top-view of $GlnA_1$ hexamer, 2-OG and substrate binding sites
756 are depicted for one horizontal dimer.

757
758 **Figure 5: Comparison of 2-OG and substrate binding site of 2-OG bound, apo and TS structures**
759 (Schumacher et al., 2023)**.** Atomic models in cartoon, important residues shown in stick
760 representation. Colors: blue/green, purple/ochre and red/yellow represent *M. mazei* $GlnA_1$ 2-OG, *M.*
761 *mazei* $GlnA_1$ apo (PDB: 8tfb, Schumacher et al., 2023) and *M. mazei* $GlnA_1$ Met-Sox-P·ADP (PDB: 8tfk,
762 Schumacher et al., 2023) transition state ($GlnA_1$ TS), respectively. **A** *left:* $GlnA_1$ 2-OG dimer in
763 superposition with $GlnA_1$ apo showing large scale movements upon 2-OG binding. **A** *right:* Close-up
764 of 2-OG binding site of $GlnA_1$ 2-OG in superposition with $GlnA_1$ apo. Dramatic movement of Helix α3
765 (residue 167-181) and R87 loop show effect of 2-OG binding. **B**: Close-up of substrate binding site of
766 $GlnA_1$ 2-OG in superposition with $GlnA_1$ apo and ADP ligand from $GlnA_1$ TS. Helix α3 movement upon
767 2-OG binding leads to a cascade of conformational changes of the phenylalanines F184, F202 and
768 F204 that lead to a priming of the active site for ATP binding. **C**: Close-up of substrate binding site of
769 $GlnA_1$ 2-OG in superposition with $GlnA_1$ TS shows high similarity between 2-OG bound and transition
770 state structure. **D**: Close-up of substrate binding site of $GlnA_1$ 2-OG in superposition with $GlnA_1$ apo
771 and Met-Sox-P ligand from $GlnA_1$ TS. Large structural changes of the D50-loop with ejection of the
772 R66 key-residue shown. Flipping of the loop allows R319 and D57 to move in further and catalyze

773 phosphoryl-transfer and attack of NH_4^+, respectively. **E**: Close-up of the substrate binding site of
774 $GlnA_1$ 2-OG in in superposition with $GlnA_1$ TS reveals strong similarity between 2-OG bound and
775 transition state structure in the active site.

776

777 **Figure 6: Feedback inhibition of $GlnA_1$ by glutamine. A**: Specific activity of purified strep-tagged
778 $GlnA_1$ (wt) and the respective R66A-mutant protein was determined as described in Materials and
779 Methods in the presence of 12.5 mM 2-OG and after additional supplementation of 5 mM glutamine.
780 For wt and the R66A-mutant one out of two biological independent replicates are exemplarily
781 shown, the deviation indicates the average of four technical replicates. **B:** Superposition GS
782 structures without glutamine of *M. mazei* (blue, green) and *B. subtilis* (orange, pink; PDB: 4lnn,
783 Murray et al., 2013): substrate binding-site including R'66 (R'62, respectively), which are responsible
784 for feedback inhibition. **C**: Exemplary mass spectra of Strep-$GlnA_1$ with 12.5 mM 2-OG in presence
785 and absence of 5 mM glutamine. The molecular masses shown above the peaks correspond to a
786 Gaussian fit of the respective peak (Gaussian fit not shown).

787

788 **Figure 7: Model of the various molecular mechanisms of glutamine synthetase activity regulation.**
789 Comparison of the regulation of glutamine synthetase activity in *E. coli /Salmonella typhimurium*, and
790 *B. subtilis, Synechocystis* and *M. mazei*. GS are in general active in a dodecameric, unmodified
791 complex under nitrogen limitation. Upon an ammonium upshift, GS are inactivated by feedback
792 inhibition (BcGS, *E. coli),* covalent modification (adenylylation, EcGS) or binding of (small) inactivating
793 proteins (*Synechocystis*, BsGS). *M. mazei* GS on the contrary is regulated via the assembly of the
794 active dodecamer upon 2-OG-binding and furthermore is strongly feedback inhibited by glutamine.
795 (Bolay et al., 2018; Klähn et al., 2018, 2015; Stadtman, 2001; Travis et al., 2022b)**.** Created with
796 BioRender.com

797

798

799 **FIGURE LEGENDS SUPPLEMENT**

800 **Figure S1: Affinity-purified Strep-$GlnA_1$ and size-exclusion-chromatography (SEC) of Strep-$GlnA_1$**
801 **after purification. A**: 1.5 µg (lane 1) and 3 µg (lane 2) Strep-$GlnA_1$ on a coomassie-stained 12 % SDS-
802 Gel. **B**: Elution profile of Strep-$GlnA_1$ (black) and size standard (dashed line, molecular weights in
803 italics). Size exclusion chromatography was performed on a Superose™ 6 Increase 10/300 GL column
804 (Cytiva, Marlborough, USA) with a flow rate of 0.5 ml/min.

805 **Figure S2: Sigmoidal fitted curves for mass photometry measurements of Strep-GlnA$_1$ with varying**
806 **concentrations of 2-OG.** The curves were fitted and K_D-values calculated using RStudio (RStudio
807 Team (2020). RStudio: Integrated Development for R. RStudio, PBC, Boston, MA URL). **A, B**: Two
808 replicates for 2-OG titration, formation of dodecamer is shown in percent. **C, D**: 2-OG titration in the
809 absence (C) and presence of GlnK$_1$ (D), formation of dodecamer is shown as a ratio of
810 dodecamer/dimer.

811 **Figure S3: Cryo-EM Data processing workflow A**: Representative motion-corrected micrograph
812 showing different orientations of the GlnA$_1$ particles **B**: Cryo-EM processing tree used for obtaining
813 the high-resolution structure of GlnA$_1$. The map obtained is coloured by resolution, where the global
814 resolution was estimated using GSFSC **C**: Different regions of GlnA$_1$ encased around the cryo-EM
815 density.

816 **Figure S4: Mass photometry of purified and thawed Strep-GlnA$_1$ before and after SEC.** Mass spectra
817 of Strep-GlnA$_1$ samples with 0 and 12.5 mM after affinity-purification (blue ●, 0 mM and green ●,
818 12.5 mM 2-OG) and after SEC (0 mM 2-OG, grey ●).
819

820 **Figure S5: Amino-acid sequence alignment of different model organism glutamine synthetases.**
821 (Alignment tool: COBALT, visualization in SnapGene) Conserved amino-acids are highlighted in green.
822 The relevant residues in *M. mazei* for 2-OG- and substrate-binding, as well as the arginine
823 responsible for the feedback inhibition by glutamine are highlighted by coloured boxes (blue ●,
824 orange ● and purple ●, respectively).
825

826 **Figure S6: *M. mazei* GlnA$_1$ filaments. A**: Representative motion-corrected micrograph showing GlnA$_1$
827 filaments **B**: Reference-free 2D classes showcasing filament orientations **C, D**: 3D reconstructed map
828 of GlnA$_1$ filament and its model.
829
830
831
832

833 **SUPPLEMENTARY TABLES**

834 **Table S1: Strains and plasmids.**

	Properties	Reference
Strains		
E. coli DH5α	General cloning strain	(Hanahan, 1983)
E. coli BL21 (DE3)	Strain for protein expression	Thermo Fisher Scientific, Waltham, USA
E. coli BL21 (DE3) + pRIL	Strain for protein expression of genes with unusual codons/ Cm^R	Stratagene, La Jolla, USA
Plasmids		
pET21a	General cloning vector providing a C-terminal His_6-tag	Novagen/Merck, Darmstadt, Germany
pETSUMO	Expression vector providing an N-terminal His_6-SUMO-tag	Thermo Fisher Scientific, Waltham, USA
pRS375	pET28a/Strep + $GlnA_1$	(Gutt et al., 2021)
pRS1672	pETSUMO + $GlnK_1$	This work
pRS1728	pEX-A258 + codon-optimized $GlnA_1$ and sP26	Eurofins Scientific, Ebersberg, Germany
pRS1841	pRS375 + codon-optimized $GlnA_1$	This work
pRS1863	pET21a + codon-optimized sP26	This work
pRS1951	pRS1840mut: R66A$GlnA_1$	This work

835

836

Table S2: Cryo-EM data collection, refinement and validation statistics

	Dodecamer Gln complex (EMDB- 19730) (PDB 8S59)
Data collection and processing	
Magnification	165,000 x
Voltage (kV)	300
Electron exposure (e–/Å^2)	55.0
Defocus range (μm)	0.25-2.0
Pixel size (Å)	0.72
Symmetry imposed	D6
Initial particle images (no.)	1,243,001
Final particle images (no.)	878,308
Map resolution (Å)	2.39
FSC threshold	0.143
Map resolution range (Å)	2.3-3.0
Refinement	
Initial model used (PDB code)	*de novo*, AlphaFold
Model resolution (Å)	2.5
FSC threshold	0.5
Model resolution range (Å)	2.2-2.5
Map sharpening *B* factor (Å^2)	-80.1
Model composition	
Non-hydrogen atoms	46968
Protein residues	5352
Ligands	AKG: 12
B factors (Å^2)	
Protein	16.58
Ligand	15.64
R.m.s. deviations	
Bond lengths (Å)	0.003
Bond angles (°)	0.602
Validation	
MolProbity score	1.29
Clashscore	5.32
Poor rotamers (%)	0.46
Ramachandran plot	
Favored (%)	98.22
Allowed (%)	1.56
Disallowed (%)	0.23

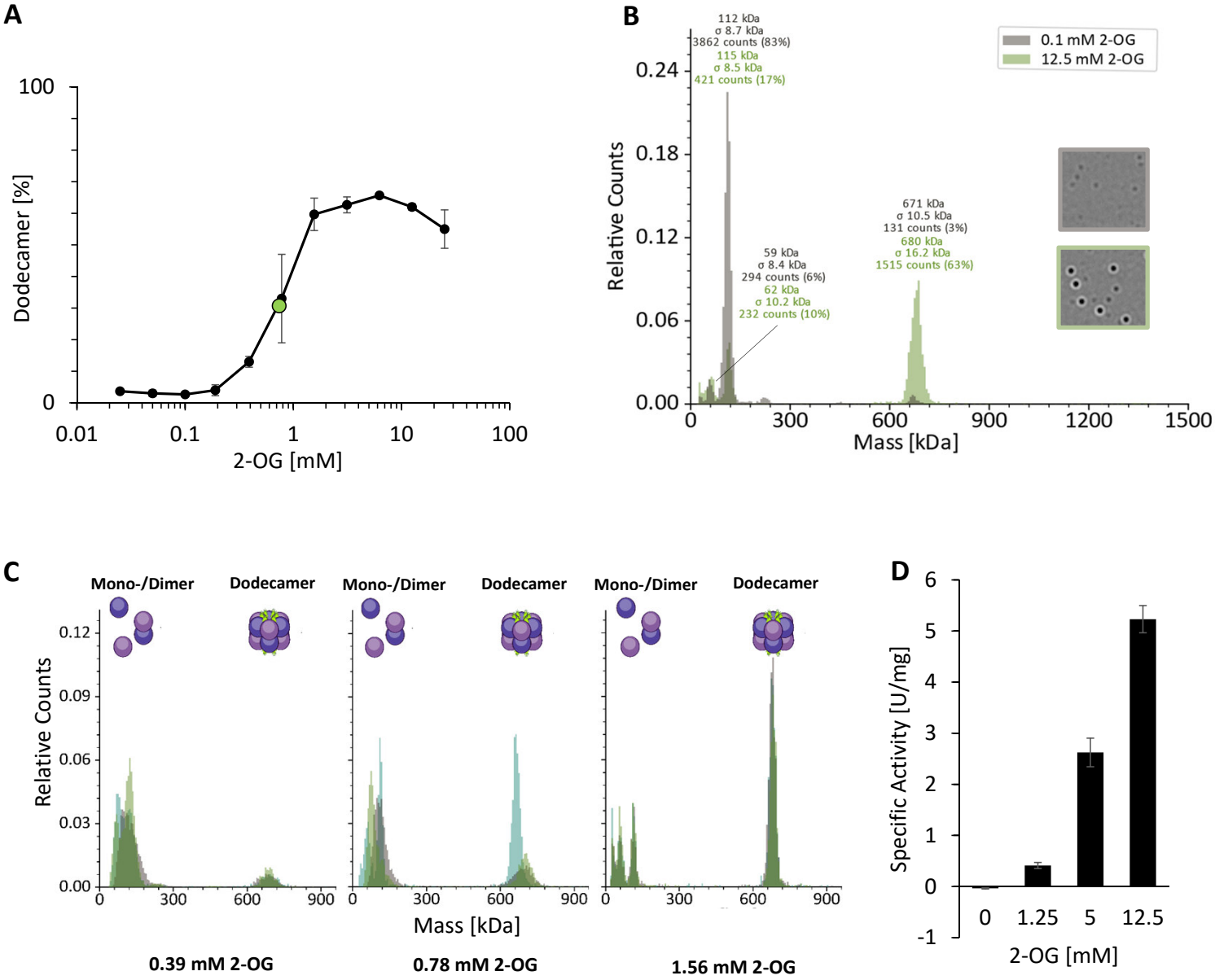
A
100
0
Dodecamer [%]
0.01
0.1
1
10
100
2-OG [mM]
B
112 kDa
σ 8.7 kDa
3862 counts (83%)
115 kDa
σ 8.5 kDa
421 counts (17%)
59 kDa
σ 8.4 kDa
294 counts (6%)
62 kDa
σ 10.2 kDa
232 counts (10%)
671 kDa
σ 10.5 kDa
131 counts (3%)
680 kDa
σ 16.2 kDa
1515 counts (63%)
0.1 mM 2-OG
12.5 mM 2-OG
Relative Counts
0.24
0.18
0.12
0.06
0.00
0
300
600
900
1200
1500
Mass [kDa]
C
Mono-/Dimer
Dodecamer
Mono-/Dimer
Dodecamer
Mono-/Dimer
Dodecamer
Relative Counts
0.12
0.09
0.06
0.03
0.00
0
300
600
900
Mass [kDa]
0.39 mM 2-OG
0.78 mM 2-OG
1.56 mM 2-OG
D
Specific Activity [U/mg]
6
5
4
3
2
1
0
-1
0
1.25
5
12.5
2-OG [mM]

Figure 1

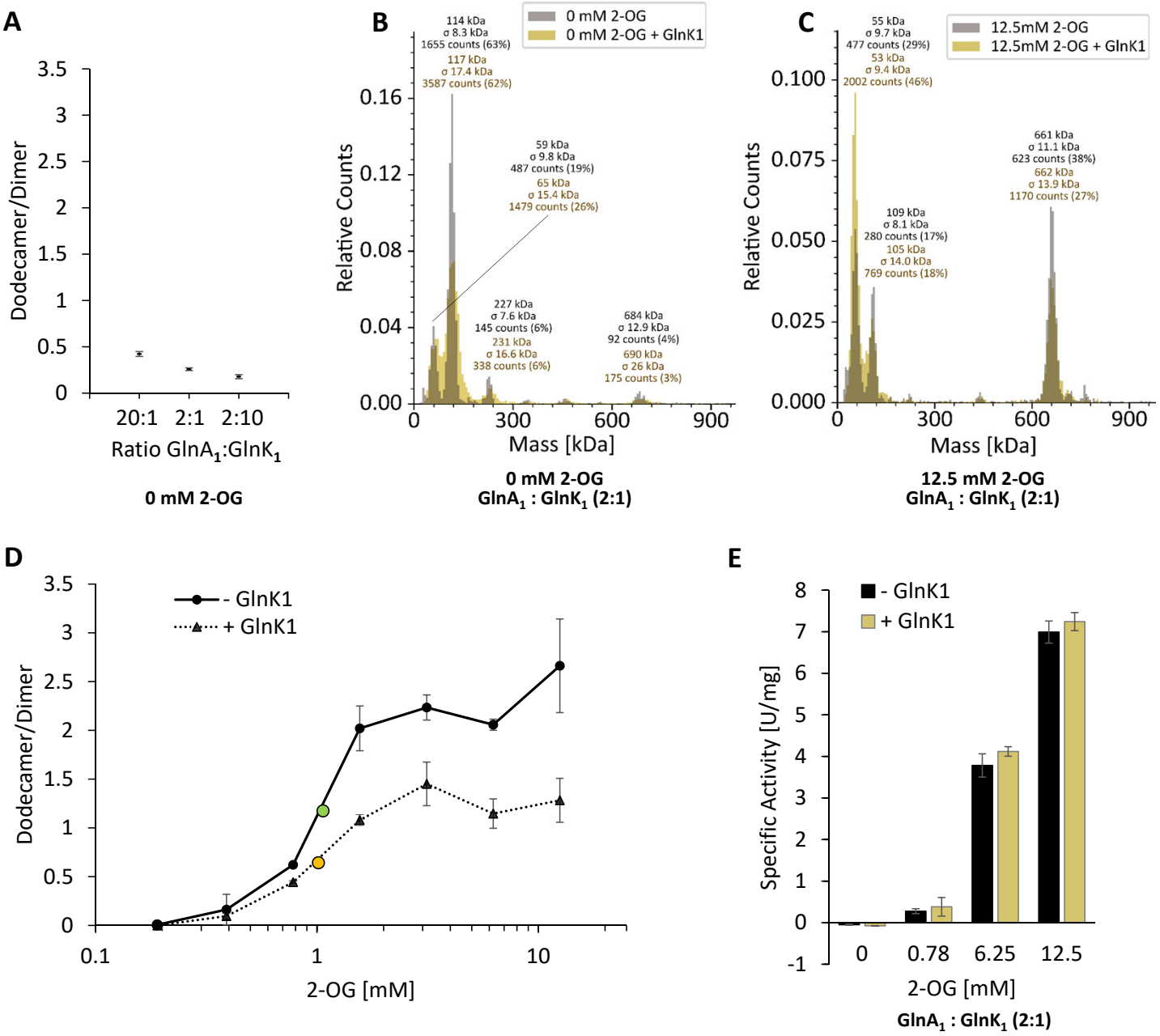
A
Dodecamer/Dimer
3.5
3
2.5
2
1.5
1
0.5
0
20:1
2:1
2:10
Ratio GlnA1:GlnK1
0 mM 2-OG
B
0 mM 2-OG
0 mM 2-OG + GlnK1
114 kDa
σ 8.3 kDa
1655 counts (63%)
117 kDa
σ 17.4 kDa
3587 counts (62%)
59 kDa
σ 9.8 kDa
487 counts (19%)
65 kDa
σ 15.4 kDa
1479 counts (26%)
227 kDa
σ 7.6 kDa
145 counts (6%)
231 kDa
σ 16.6 kDa
338 counts (6%)
684 kDa
σ 12.9 kDa
92 counts (4%)
690 kDa
σ 26 kDa
175 counts (3%)
Relative Counts
0.16
0.12
0.08
0.04
0.00
0
300
600
900
Mass [kDa]
0 mM 2-OG
GlnA1 : GlnK1 (2:1)
C
12.5mM 2-OG
12.5mM 2-OG + GlnK1
55 kDa
σ 9.7 kDa
477 counts (29%)
53 kDa
σ 9.4 kDa
2002 counts (46%)
109 kDa
σ 8.1 kDa
280 counts (17%)
105 kDa
σ 14.0 kDa
769 counts (18%)
661 kDa
σ 11.1 kDa
623 counts (38%)
662 kDa
σ 13.9 kDa
1170 counts (27%)
Relative Counts
0.100
0.075
0.050
0.025
0.000
0
300
600
900
Mass [kDa]
12.5 mM 2-OG
GlnA1 : GlnK1 (2:1)
D
- GlnK1
+ GlnK1
Dodecamer/Dimer
3.5
3
2.5
2
1.5
1
0.5
0
0.1
1
10
2-OG [mM]
E
- GlnK1
+ GlnK1
Specific Activity [U/mg]
8
7
6
5
4
3
2
1
0
-1
0
0.78
6.25
12.5
2-OG [mM]
GlnA1 : GlnK1 (2:1)

Figure 2:

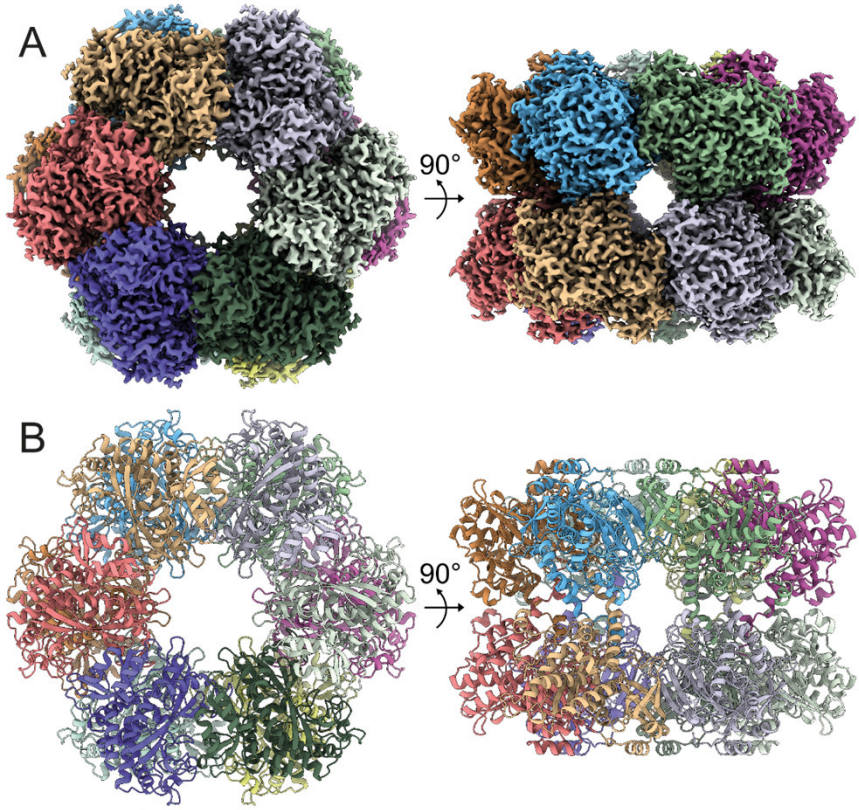

Figure 3

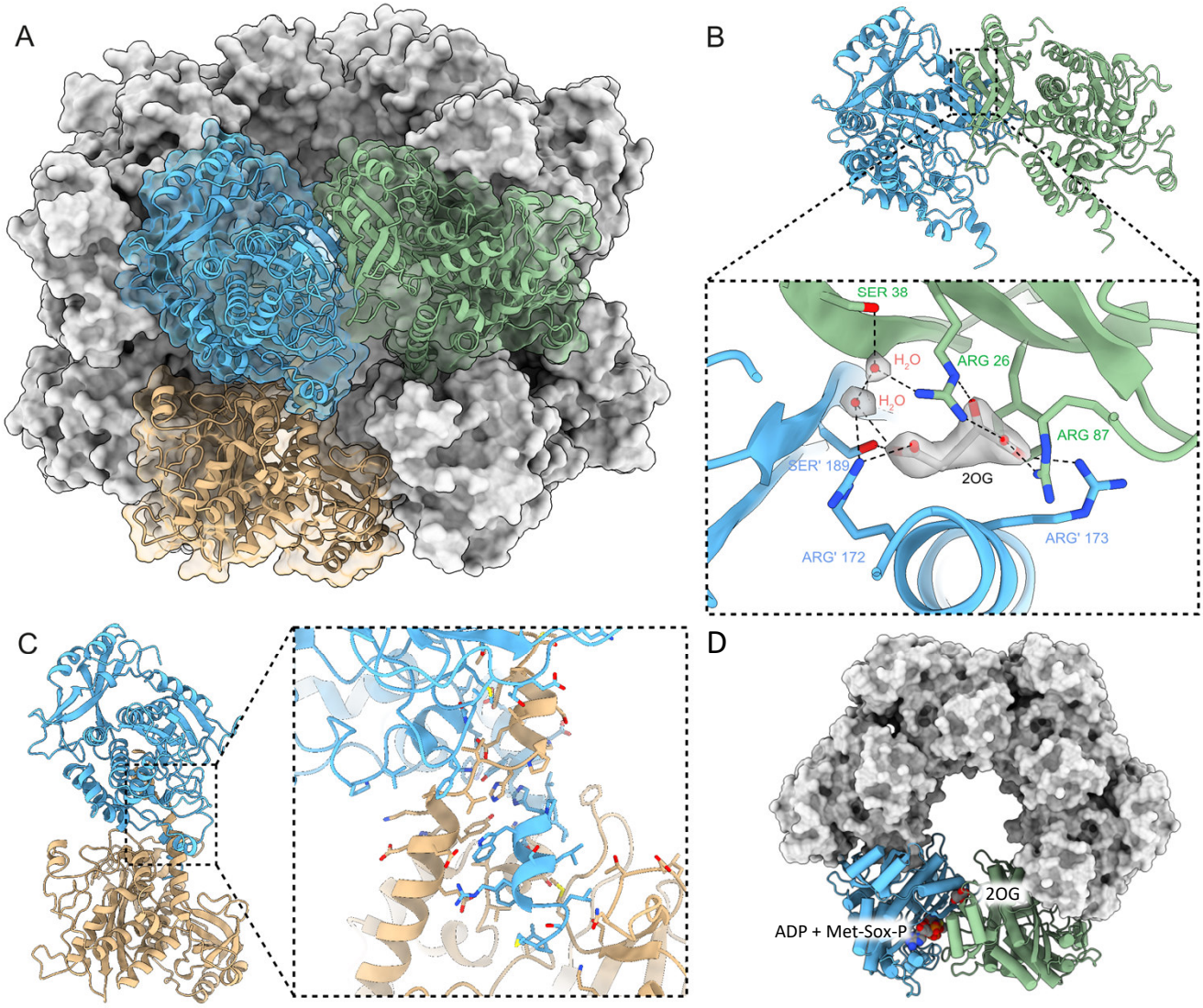
A
B
SER 38
H_2O
ARG 26
H_2O
ARG 87
SER' 189
2OG
ARG' 173
ARG' 172
C
D
2OG
ADP + Met-Sox-P

Figure 4

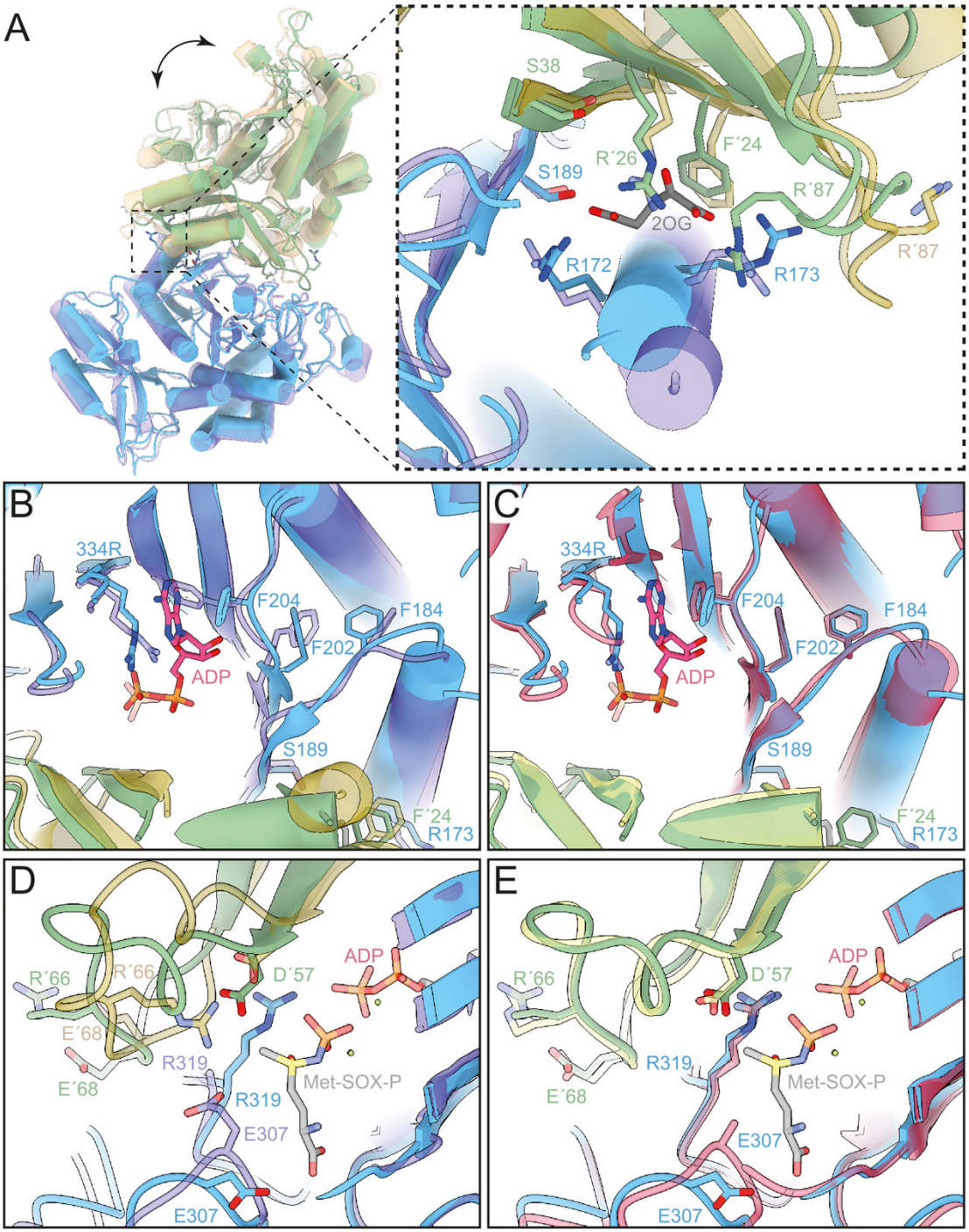
A
S38
S189
R´26
F´24
R´87
2OG
R´87
R172
R173
B
334R
F204
F184
F202
ADP
S189
F´24
R173
C
334R
F204
F184
F202
ADP
S189
F´24
R173
D
R´66
R´66
D´57
ADP
E´68
R319
E´68
R319
Met-SOX-P
E307
E307
E
R´66
D´57
ADP
R319
E´68
Met-SOX-P
E307
E307

Figure 5

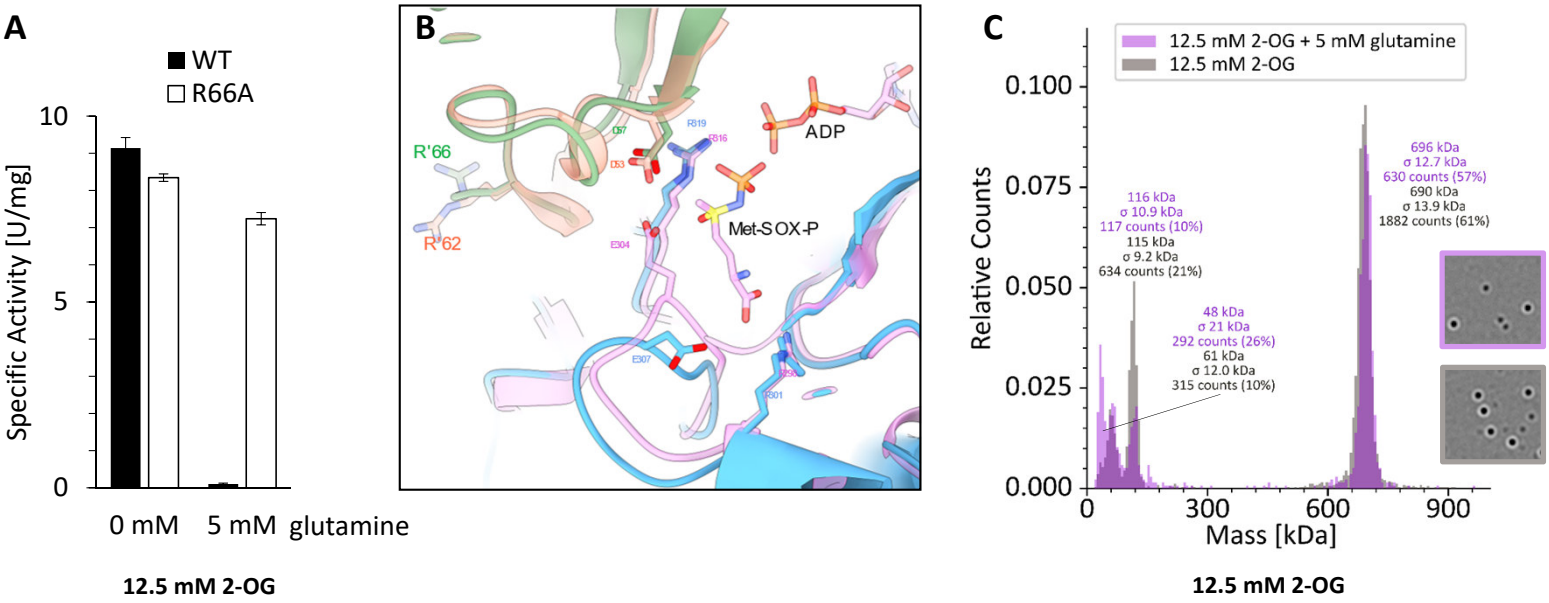
A
WT
R66A
Specific Activity [U/mg]
10
5
0
0 mM
5 mM
glutamine
12.5 mM 2-OG
B
R'66
R'62
ADP
Met-SOX-P
C
12.5 mM 2-OG + 5 mM glutamine
12.5 mM 2-OG
Relative Counts
0.100
0.075
0.050
0.025
0.000
0
300
600
900
Mass [kDa]
116 kDa
σ 10.9 kDa
117 counts (10%)
115 kDa
σ 9.2 kDa
634 counts (21%)
48 kDa
σ 21 kDa
292 counts (26%)
61 kDa
σ 12.0 kDa
315 counts (10%)
696 kDa
σ 12.7 kDa
630 counts (57%)
690 kDa
σ 13.9 kDa
1882 counts (61%)
12.5 mM 2-OG

Figure 6:

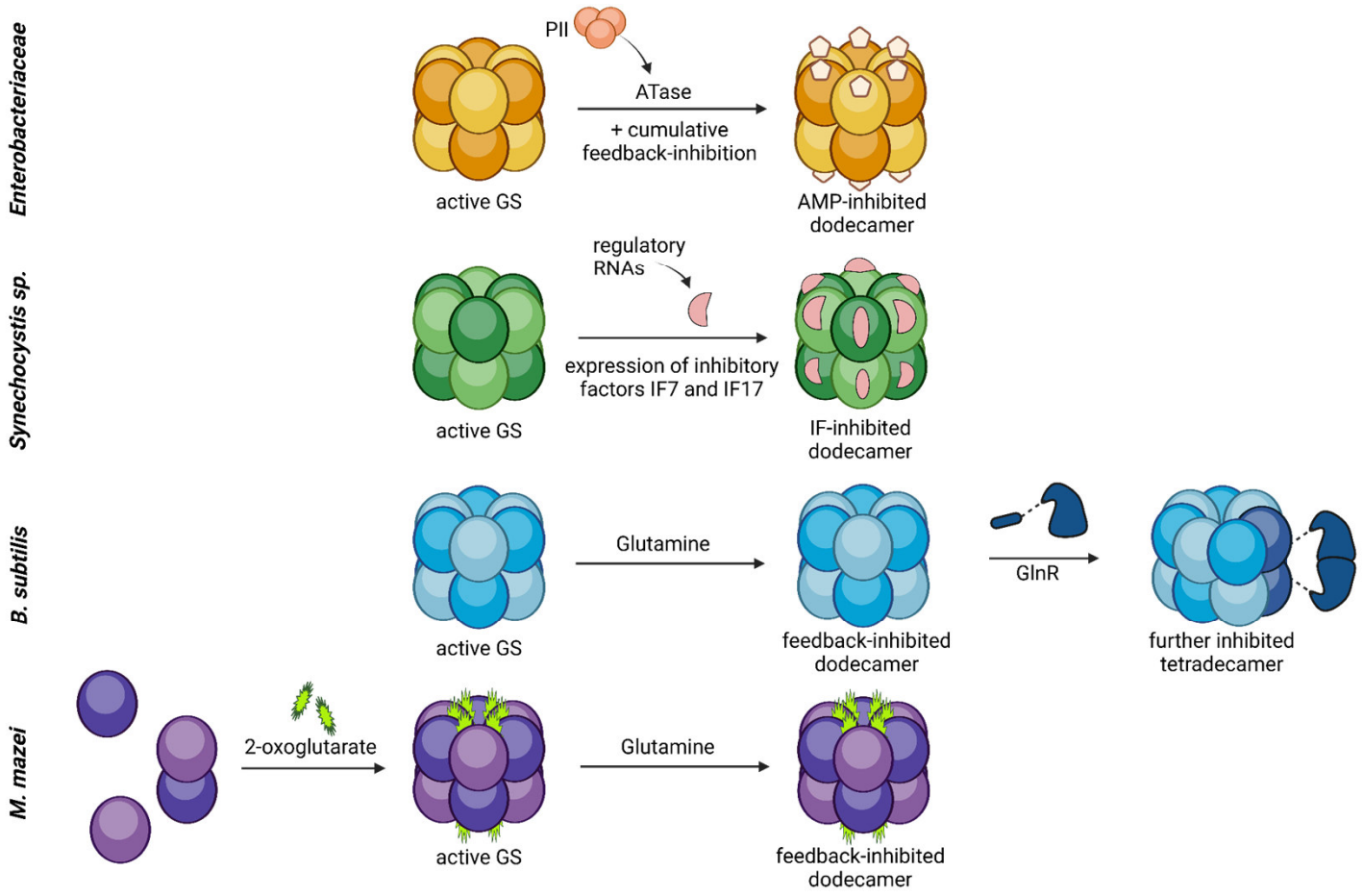
Enterobacteriaceae
PII
ATase
+ cumulative
feedback-inhibition
active GS
AMP-inhibited
dodecamer
Synechocystis sp.
regulatory
RNAs
expression of inhibitory
factors IF7 and IF17
active GS
IF-inhibited
dodecamer
B. subtilis
Glutamine
GlnR
active GS
feedback-inhibited
dodecamer
further inhibited
tetradecamer
M. mazei
2-oxoglutarate
Glutamine
active GS
feedback-inhibited
dodecamer

Figure 7: